# LES in the Surface Layer: Surface Fluxes, Scaling, and SGS Modeling

J. C. WYNGAARD,* L. J. PELTIER,+ AND S. KHANNA

*Department of Meteorology, The Pennsylvania State University, University Park, Pennsylvania*

(Manuscript received 9 January 1996, in final form 27 August 1997)

ABSTRACT

The surface fluxes in the fine-mesh numerical codes used in small-scale meteorology are typically diagnosed from resolvable-scale variables through surface-exchange coefficients. This is appropriate if the aspect ratio (length/height) of the grid volume adjacent to the surface is very large, as in mesoscale models. The aspect ratio can approach unity in large-eddy simulation (LES) codes for the planetary boundary layer, however. In that limit the surface-exchange coefficients are random variables, and it is shown through analysis of surface-layer measurements and LES results that their fluctuation levels can be large.

As an alternative to surface-exchange coefficients, the authors derive conservation equations for the surface scalar and momentum fluxes in LES. Scaling relations for resolvable-scale variables in the surface layer are developed and used to simplify these equations. It is shown that, as the grid aspect ratio decreases toward unity, local time change, horizontal advection, production due to horizontal velocity convergence, and random noise terms cause the local surface-exchange coefficients to fluctuate. A simple closure of the equations is adopted, which has little effect on surface-layer structure calculated through LES with a Smagorinsky-based subgrid-scale (SGS) model. Through analysis of very high-resolution LES fields, the authors find the SGS model to be a poor representation of surface-layer physics and conclude that the surface-flux conservation equations need to be coupled with a greatly improved SGS model in the surface layer.

## 1. Introduction

Large-eddy simulation, or LES, is now very widely used in small-scale meteorology. Applications range from severe storms (Klemp 1987) to small-mesoscale phenomena (Cotton et al. 1993) and boundary layer meteorology (Moeng 1984; Mason and Thomson 1987; Nieuwstadt et al. 1993; Schumann 1993).

The strength of LES lies in its explicit calculation of the energy-containing eddies of a turbulent flow. The unresolvable or subgrid-scale (SGS) eddies, which are formally removed by spatial filtering of the governing equations (Leonard 1974), manifest themselves through SGS terms in the filtered or resolvable-scale equations. If the scale of the filter is small compared to the scale of the energy-containing eddies, the resolvable-scale eddies do contain most of the turbulent kinetic energy and fluxes. Furthermore, they are fairly insensitive to the details of the SGS model used to close the filtered equations. Thus, well-resolved LES has an appealing robustness.

Because the horizontal length scale of the vertical velocity fluctuations scales with distance from the surface, LES inevitably has inadequate spatial resolution near the surface. As a result, the SGS model takes on much more importance there than in other regions of the flow. Furthermore, the specification of resolvable-scale surface fluxes comes into question since the widely used surface-exchange coefficients are not obviously valid locally. Thus, the fidelity of LES within the surface layer is problematic.

In this paper we study three closely related aspects of LES in the surface layer. First we examine the behavior of the surface-exchange coefficients when the grid aspect ratio (horizontal dimension/vertical dimension) is of order 1, as in LES. As an alternative to surface-exchange coefficients, we develop conservation equations for the resolvable-scale surface fluxes. Simplifying these surface-flux equations requires our second development, scaling relations for LES variables in the surface layer. These determine how turbulent variances are apportioned between the resolvable and SGS components. Finally, in order to interpret the impact of the resolvable-scale surface-flux equations on LES fields we evaluate some aspects of the performance of the widely used eddy-diffusivity SGS model in the surface layer.

* Also Department of Mechanical Engineering, The Pennsylvania State University, University Park, Pennsylvania.

+ Current affiliation: Applied Research Laboratory, The Pennsylvania State University, University Park, Pennsylvania.

*Corresponding author address:* Dr. John C. Wyngaard, Department of Meteorology, 503 Walker Building, The Pennsylvania State University, University Park, PA 16802-5013.
E-mail: wyngaard@ems.psu.edu

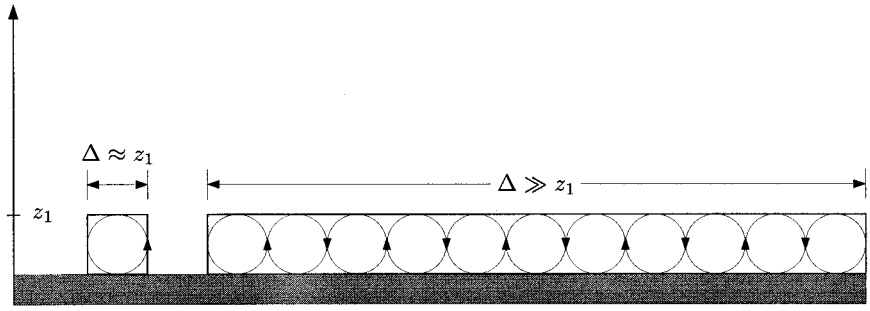


FIG. 1. A schematic of the ''coupling eddies'' in the grid volume adjacent to the surface. They couple the resolvable-scale flow at height $z_1$ to the SGS surface flux. For a unity aspect ratio grid (left) there is only one such coupling eddy; for a large aspect ratio (right) there are many.

## 2. Surface-exchange coefficients for resolvable-scale fluxes

### a. Background

The LES codes used in boundary layer meteorology (e.g., Nieuwstadt et al. 1993) involve the surface fluxes of momentum, temperature, water vapor, and trace constituents. Since these codes use local spatial averaging of the governing equations rather than ensemble averaging, these are *resolvable-scale* surface fluxes that contain not only the ensemble mean but also the fluctuations about this mean on scales up to the filter cutoff. Most such codes take this resolvable-scale surface flux as proportional to the product of the horizontal wind speed and the difference in the transported quantity between the surface and the first grid point. The proportionality factor is the surface-exchange coefficient.

Surface-exchange coefficients for ensemble-average fluxes under horizontally homogeneous conditions are known from several decades of surface-layer research. In coarse-resolution (e.g., mesoscale) models, the horizontal scale $\Delta$ of the local spatial averaging and of the numerical grid is typically much larger than the height $z_1$ of the first grid level. The *grid aspect ratio* $\Delta/z_1$ is large, meaning that there are many ''coupling eddies'' in the first grid volume, as illustrated in Fig. 1. In this case these *mean* exchange coefficients, as we will call them, are applicable. In LES, however, the grid aspect ratio is typically in the range from 1 to 3; there are not many coupling eddies and the surface-exchange coefficient has a random component. Thus, for $\tilde{F}^r_0(x_1, x_2, t)$, the resolvable-scale surface flux of a scalar constituent, for example, the appropriate surface-exchange coefficient is not the mean value $C_H$ but a random variable, $\tilde{C}_H$. (A superscript $r$, for resolvable scale, indicates that the variable has been spatially filtered; a tilde denotes that it has both mean and fluctuating parts.) Thus, the expression for surface flux is more properly written as

$$\tilde{F}^r_0(x_1, x_2, t) = \tilde{C}_H(x_1, x_2, z_1, t)[\tilde{u}^r_1(x_1, x_2, z_1, t)\Delta\tilde{c}^r(x_1, x_2, z_1, t)]^r. \quad (1)$$

Here $\tilde{u}^r_1$ and $\Delta\tilde{c}^r$ are the streamwise components of resolvable-scale wind at the first grid level and the resolvable-scale $\tilde{c}$ difference between the first grid point and the surface, respectively. We call $\tilde{C}_H$ the *local* surface-exchange coefficient; we expect that $\tilde{C}_H \to C_H$ as $z_1/\Delta \to 0$.

### b. Observed fluctuations in local surface-exchange coefficients

Consider two LES grids of horizontal spacing $\Delta$, in one the first grid point being close to the surface, at $z_s \ll \Delta$, and in the other at a greater height $z_1 \approx \Delta$. In view of these grid aspect ratios, we take the scalar-flux surface-exchange coefficients as $C_H(z_s)$ for the first grid and $\tilde{C}_H(z_1)$ for the second. We can write from (1), indicating only the $z$ dependence,

$$\tilde{F}^r_0 = C_H(z_s)[\tilde{u}^r_1(z_s)\Delta\tilde{c}^r(z_s)]^r = \tilde{C}_H(z_1)[\tilde{u}^r_1(z_1)\Delta\tilde{c}^r(z_1)]^r. \quad (2)$$

Solving for the local surface-exchange coefficient at height $z_1$ yields

$$\tilde{C}_H(z_1) = C_H(z_s)\frac{[\tilde{u}^r_1(z_s)\Delta\tilde{c}^r(z_s)]^r}{[\tilde{u}^r_1(z_1)\Delta\tilde{c}^r(z_1)]^r}. \quad (3)$$

We decompose the resolvable-scale fields into the sum of the ensemble mean and a fluctuating part, using upper case symbols for the former:

$$\tilde{u}^r_i = U_i + u^r_i, \qquad \tilde{c}^r = C + c^r, \qquad \Delta\tilde{c}^r = \Delta C + \Delta c^r. \quad (4)$$

Using the decomposition (4) and expanding (3) yields

$$\tilde{C}_H(z_1) = C_H(z_s)\frac{\Delta C(z_s)U_1(z_s)}{\Delta C(z_1)U_1(z_1)} \times \frac{\left[\left(1 + \dfrac{\Delta c^r(z_s)}{\Delta C(z_s)}\right)\left(1 + \dfrac{u^r_1(z_s)}{U_1(z_s)}\right)\right]^r}{\left[\left(1 + \dfrac{\Delta c^r(z_1)}{\Delta C(z_1)}\right)\left(1 + \dfrac{u^r_1(z_1)}{U_1(z_1)}\right)\right]^r}. \quad (5)$$

We evaluated (5) using LES data for the convective boundary layer and observations from the STORMFEST experiment. The LES domain was 5 km × 5 km in the horizontal and 2 km deep. It used a nested mesh in the surface layer so the resolution there was equivalent to that of a $256^3$ simulation (Khanna and Brasseur 1996). The inversion height $z_i$ was about 1000 m. In one run the geostrophic wind was 5.0 m $s^{-1}$ and the surface temperature flux was 0.14 m $s^{-1}$ K, giving $-z_i/L = 63$. The other run had a geostrophic wind of 1.0 m $s^{-1}$ and a surface temperature flux of 0.24 m $s^{-1}$ K, giving $-z_i/L = 730$. We took $z_s = 3.9$ m, the lowest grid point, and evaluated the local surface-exchange coefficients at $z_1 = 12$ and 27 m, using temperature as the scalar.

The STORMFEST data, taken by the NCAR Atmospheric Surface Transfer and Exchange Research facility, included time series of fluctuating temperature and the horizontal components of velocity from in situ sensors at $z = 1$ m, 4 m, and 10 m. The mean wind speed at 10 m was 10.7 m $s^{-1}$, the surface temperature flux was 0.23 m $s^{-1}$ K, the Monin–Obukhov length $L$ was $-63$ m, and $-z_i/L \approx 10$. We took $z_s = 1.0$ m, the lowest measurement point, and evaluated the local surface-exchange coefficients for temperature at $z_1 = 4$ m and 10 m.

The randomness factor in (5) involves wave-cutoff filtering at wavenumber magnitude $\kappa_c$ in the horizontal wavenumber plane. We did this straightforwardly with the LES data, using several values of $\kappa_c = \pi/\Delta$. This gave $z_s/\Delta \leq 0.13$. For the STORMFEST data we approximated the averaging by wave-cutoff filtering of the time series at frequency $\omega_c$, using Taylor's hypothesis in the form $\kappa_c = \omega_c/U$. Here $z_s/\Delta \leq 0.10$.

Figure 2 shows the fluctuations in the local surface-exchange coefficient $\tilde{C}_H$ and its counterpart for momentum, $\tilde{C}_D$, evaluated from measured time series and LES data, using (5) and its counterpart for $\tilde{C}_D$. The fluctuation level increases as grid aspect ratio decreases, as we anticipated through the coupling-eddies notion depicted in Fig. 1, and it increases as $-z_i/L$ increases. It can be quite large.

As discussed by Wyngaard and Peltier (1996), we can gain insight into the fluctuations of the local surface-exchange coefficient through a simple model of Eq. (5). If $\Delta c^r/\Delta C$ and $u_1^r/U_1$ are small parameters, we can linearize (5) to find

$$\tilde{C}_H(z_1) = C_H(z_s)\frac{\Delta C(z_s)U_1(z_s)}{\Delta C(z_1)U_1(z_1)} \times \left(1 + \frac{\Delta c^r(z_s)}{\Delta C(z_s)} + \frac{u_1^r(z_s)}{U_1(z_s)} - \frac{\Delta c^r(z_1)}{\Delta C(z_1)} - \frac{u_1^r(z_1)}{U_1(z_1)}\right). \quad (6)$$

Taking the ensemble mean gives

$$\overline{\tilde{C}_H}(z_1) = C_H(z_s)\frac{\Delta C(z_s)U_1(z_s)}{\Delta C(z_1)U_1(z_1)} = C_H(z_1), \quad (7)$$

which indicates that for small fluctuation levels the mean of the local surface-exchange coefficient is the traditional surface-exchange coefficient. For sufficiently large fluctuation levels the two can differ. In the convective surface layer the fluctuation level of $\Delta c^r/\Delta C$ is typically much less than that of $u_1^r/U_1$, so that we can write (6) as

$$\tilde{C}_H(z_1) \approx C_H(z_1)\left(1 + \frac{u_1^r(z_s)}{U_1(z_s)} - \frac{u_1^r(z_1)}{U_1(z_1)}\right), \quad (8)$$

which implies that

$$\frac{\overline{(\tilde{C}_H(z_1) - C_H(z_1))^2}}{C_H^2(z_1)} \approx \overline{\left(\frac{u_1^r(z_s)}{U_1(z_s)} - \frac{u_1^r(z_1)}{U_1(z_1)}\right)^2}. \quad (9)$$

As $\Delta/z_1$ becomes large, the separation $z_1 - z_s$ becomes small compared to the horizontal scales of the fluctuations in $u_1^r/U_1$. Thus, as $\Delta/z_1$ increases, we expect $u_1^r(z_s)$ and $u_1^r(z_1)$ to become increasingly well correlated and their rms difference to decrease; from (9) the fluctuation level in the local surface-exchange coefficient should then approach zero. This is consistent with the results in Fig. 2.

This suggests that the surface-exchange coefficient fluctuations are due to the decreasing correlation between resolvable-scale fields very near the surface and at $z_1$ as $\kappa_c z_1 \to 1$. Further analysis of these LES and STORMFEST data by Wyngaard and Peltier (1996) supports this notion.

An alternative to treating the resolvable-scale surface fluxes through surface-exchange coefficients is predicting them directly through their conservation equations. We discuss this next, focusing on the scalar flux. We treat the momentum flux in appendix C.

## 3. The subgrid-scale flux near the surface

The Boussinesq equations for velocity $\tilde{u}_i$ and a conservative scalar $\tilde{c}$ in the surface layer are

$$\frac{\partial \tilde{u}_i}{\partial t} + \tilde{u}_{i,j}\tilde{u}_j = -\tilde{p}_{,i} + \frac{g}{T_0}\tilde{\theta}\delta_{3i} + \nu\tilde{u}_{i,jj}, \qquad \tilde{u}_{i,i} = 0, \quad (10)$$

$$\frac{\partial \tilde{c}}{\partial t} + (\tilde{c}\tilde{u}_j)_{,j} = \gamma\tilde{c}_{,jj}, \quad (11)$$

where $\tilde{p}$ is kinematic pressure, $\gamma$ is the molecular dif-

fusivity of $\tilde{c}$, and $\theta$ is potential temperature (Lumley and Panofsky 1964; Stull 1988). We assume Coriolis effects are negligible. We spatially low-pass filter each field over horizontal planes (Leonard 1974), designating the part that passes through the filter as *resolvable* and the remainder as *subgrid scale*, denoted with superscripts $r$ and $s$, respectively. This yields the decomposition

$$\tilde{u}_i = \tilde{u}_i^r + \tilde{u}_i^s, \qquad \tilde{c} = \tilde{c}^r + \tilde{c}^s,$$
$$\tilde{\theta} = \tilde{\theta}^r + \tilde{\theta}^s, \qquad \tilde{p} = \tilde{p}^r + \tilde{p}^s. \tag{12}$$

We assume that in horizontal wavenumber space the filter has a sharp cutoff at wavenumber magnitude $\kappa_c = \pi/\Delta^f$, where $\Delta^f$ is the filter width in physical space. In principle $\Delta^f$ need not be the same as $\Delta^g$, the horizontal grid spacing. As pointed out by Mason and Callen (1986), $\Delta^f$ defines the spatial scales contained in the resolvable fields, whereas $\Delta^g$ determines the accuracy of the numerical solutions of the filtered equations. One could obtain very high accuracy by taking $\Delta^g \ll \Delta^f$, for example. Computer limitations require that $\Delta^f$ and $\Delta^g$ be essentially the same value, however, so we will not distinguish them further here, taking $\Delta^f = \Delta^g = \Delta$. With our sharp cutoff filter the $r$ and $s$ fields have no wavenumber components in common; this implies that their covariance vanishes since nonoverlapping Fourier modes are uncorrelated (Lumley and Panofsky 1964).

Equation (11) holds for any advected scalar that is *conservative*, that is, has no sources or sinks. Filtering it yields the evolution equation for its resolvable-scale part:

$$\frac{\partial \tilde{c}^r}{\partial t} + (\tilde{c}^r \tilde{u}_j^r)_{,j}^r + (\tilde{c}^r \tilde{u}_j^s + \tilde{c}^s \tilde{u}_j^r + \tilde{c}^s \tilde{u}_j^s)_{,j}^r = \gamma \tilde{c}_{,jj}. \tag{13}$$

We write this as

$$\frac{\partial \tilde{c}^r}{\partial t} + (\tilde{c}^r \tilde{u}_j^r)_{,j}^r + \tilde{F}_{j,j}^r = 0,$$
$$\tilde{F}_j^r = (\tilde{c}^r \tilde{u}_j^s + \tilde{c}^s \tilde{u}_j^r + \tilde{c}^s \tilde{u}_j^s)^r - \gamma \tilde{c}_{,j}. \tag{14}$$

Naming $\tilde{F}_j^r$ is a challenge since it involves four terms, multiple filtering operations, and both turbulent and molecular components. The name ''resolvable-scale flux'' does not distinguish it from $(\tilde{c}^r \tilde{u}_j^r)^r$. Its molecular term is important only in a very thin layer adjacent to the surface, and each of its three remaining terms has a subgrid-scale contribution. Thus, we will call $\tilde{F}_j^r$ the subgrid-scale (SGS) flux.

The terms in (14), being resolvable scale, are bounded as $z \to 0$ (we will use $x_3$ and $z$ interchangeably to denote height above the surface). In particular, $\tilde{F}_{3,3}^r$ is bounded so that for sufficiently small $z$, $\tilde{F}_3^r(z) \approx \tilde{F}_0^r$, the resolvable-scale surface flux. Thus, we expect a ''constant-SGS-flux'' layer near the surface within which $\tilde{F}_3^r$ is a surrogate for the resolvable-scale surface flux. In section 4 we will confirm this through scaling estimates.

We decompose each resolvable-scale field into the sum of the ensemble mean and a fluctuating part, using upper case symbols for the former:

$$\tilde{u}_i^r = U_i + u_i^r, \qquad \tilde{c}^r = C + c^r, \qquad \tilde{\theta}^r = \Theta + \theta^r,$$
$$\tilde{p}^r = P + p^r, \qquad \tilde{F}_j^r = F_j + F_j^r. \tag{15}$$

Since the ensemble means of the subgrid-scale field and of the fluctuating part of the resolvable-scale field vanish, we can write

$$\tilde{u}_i^s = u_i^s, \qquad \tilde{c}^s = c^s, \qquad \tilde{\theta}^s = \theta^s, \qquad \tilde{p}^s = p^s. \tag{16}$$

At heights $z$ sufficiently large that the molecular contribution to the SGS flux is negligible the vertical component of the flux is, from (14)–(16),

$$\tilde{F}_3^r = [(C + c^r)u_3^s + c^s(U_3 + u_3^r) + c^s u_3^s]^r$$
$$= (c^r u_3^s + c^s u_3^r + c^s u_3^s)^r, \tag{17}$$

assuming a wave-cutoff filter.

We can determine the relative magnitudes of the three components of the SGS flux by using the Peltier et al. (1996) model of the two-dimensional spectrum $E(\kappa)$ in the surface layer, where $\kappa$ is horizontal wavenumber magnitude $(\kappa_1^2 + \kappa_2^2)^{1/2}$. This spectrum integrates to the variance

$$\int_0^\infty E(\kappa)\, d\kappa = \text{variance}. \tag{18}$$

They used a single form for both horizontal velocity and a conservative scalar,

$$E(\kappa) = \frac{c_1 l^2 s^2 \kappa}{[c_2 + (\kappa l)^2]^{4/3}}, \tag{19}$$

with $c_1$ and $c_2$ adjustable constants and $l$ and $s$ the length and intensity scales. For vertical velocity they multiplied this form by a transfer function that models the effects of continuity and the $u_3 = 0$ surface condition by attenuating $E(\kappa)$ at the smallest wavenumbers.

The spectrum (19) has a peak at $\kappa \sim 1/l$ and a $\kappa^{-5/3}$ inertial range asymptote at $\kappa \gg l^{-1}$. Peltier et al. chose the constants $c_1$ and $c_2$ by requiring the variance and the inertial-range spectral level to agree with observations. They chose the length and intensity scales $l$ and $s$ as $z$ and $u_*$ under neutral conditions. In free convection they chose the scales as the PBL depth $z_i$ and the convective velocity scale $w_* = (gQ_0 z_i/T_0)^{1/3}$, rather than the local-free-convection scales $z$ and $u_f = (gQ_0 z/T_0)^{1/3}$ (Wyngaard et al. 1971); here $Q_0$ is the ensemble-mean surface temperature flux. As justification they cited the evidence that horizontal velocity fluctuations in the unstable surface layer are not Monin–Obukhov (M–O) similar, but instead scale with the mixed-layer scales $z_i$ and $w_*$ (Kaimal 1978; Wyngaard 1988).

Peltier et al. then combined the neutral and free convection forms to give an interpolation formula for the entire stability range between them. The spectrum $E(\kappa)$ cannot be directly measured with conventional instru-

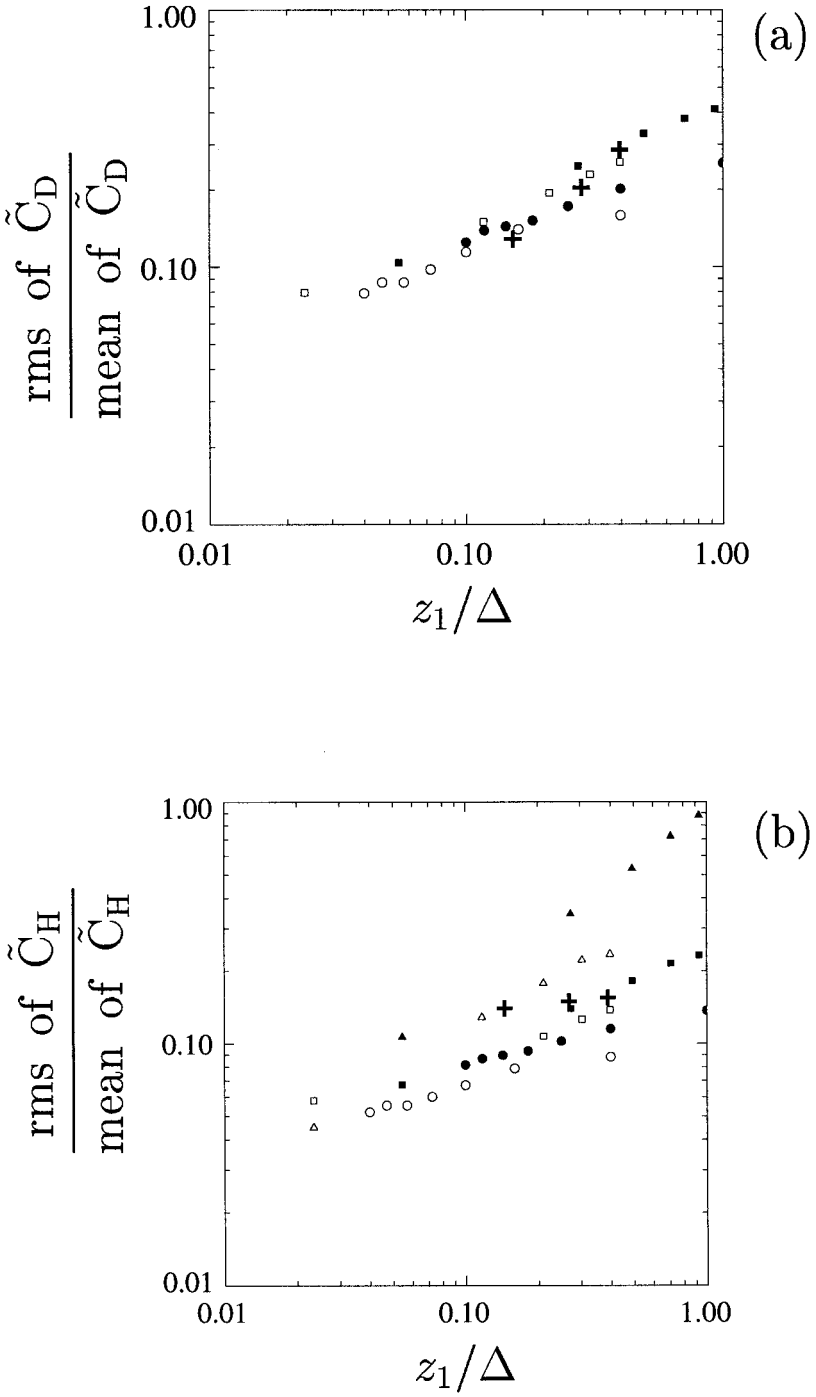


FIG. 2. Behavior of the local surface-exchange coefficients as calculated from high-resolution LES and STORMFEST data taken by the NCAR ASTER facility. Circles: STORMFEST at 4 m (open) and 10 m (solid); $-z_i/L \approx 10$. Squares: LES at 12 m (open) and 27 m (solid); $-z_i/L \approx 63$. Triangles: LES at 12 m (open) and 27 m (solid); $-z_i/L \approx 800$. Plus symbols: LES at 16 m using surface-flux equations.

ments, but Peltier et al. showed that the corresponding one-dimensional spectra agree well with existing measurements.

The modeled two-dimensional spectra are shown in Fig. 3 in area-preserving coordinates. For all but near-neutral conditions the horizontal spectrum $E_h$, which integrates to $(\overline{u_1^2} + \overline{u_2^2})/2$, peaks at wavenumbers of the order of $\kappa_h = 1/z_i$. The vertical velocity spectrum $E_v$

peaks at larger wavenumbers, those of the order of $\kappa_z = 1/z$. A third significant wavenumber is $\kappa_c = \pi/\Delta$, the cutoff wavenumber of the LES grid mesh. In Moeng's $96^3$ LES code, for example, $\Delta$ is typically 5000 m/64 $\simeq$ 80 m.

Let us now examine the contributions to the SGS flux as shown in (17) for heights $z \ll \Delta$ and inversion depths $z_i \gg \Delta$. Since $z \ll \Delta \ll z_i$, there is a large separation in these three wavenumbers: $\kappa_h \ll \kappa_c \ll \kappa_z$. Let us write each factor in the first cross term, $(c^r u_3^s)^r$, as a Fourier–Stieltjes integral, noting the admissible region in the $\kappa_1$, $\kappa_2$ plane:

$$c^r(x_i) = \int e^{i\kappa_j' x_j}\, dT(\kappa_j', |\kappa_j'| \le \kappa_c),$$
$$u_3^s(x_i) = \int e^{i\kappa_j'' x_j}\, dW(\kappa_j'', |\kappa_j''| > \kappa_c). \qquad (20)$$

It follows that

$$(c^r u_3^s)^r = \int\int_{|\kappa_j'+\kappa_j''|<\kappa_c} e^{i(\kappa_j'+\kappa_j'')x_j}\, dT(\kappa_j', |\kappa_j'| \le \kappa_c)\, dW(\kappa_j'', |\kappa_j''| > \kappa_c). \qquad (21)$$

Since $|\kappa_j'| \le \kappa_c$, the restriction $|\kappa_j' + \kappa_j''| \le \kappa_c$ implies that $|\kappa_j''| < 2\kappa_c$. Thus, only $u_3$ modes of wavenumber magnitude less than $2\kappa_c$ can contribute to $(c^r u_3^s)^r$. Figure 3 shows that, as we approach the surface, $2\kappa_c$ falls below the range of wavenumbers contributing significantly to $u_3$ so that $(c^r u_3^s)^r \to 0$ as $z/\Delta \to 0$. The second cross term in (17), $(c^s u_3^r)^r$, is also eliminated because $u_3^r \to 0$ as $z/\Delta \to 0$.

We conclude that for $z/\Delta \ll 1$ the SGS flux is due entirely to the third term in (17),

$$\tilde{F}_3^r \approx (c^s u_3^s)^r \approx \int\int_{|\kappa_j'+\kappa_j''|<\kappa_c} e^{i(\kappa_j'+\kappa_j'')x_j}\, dT(\kappa_j', |\kappa_j'| > \kappa_c)\, dW(\kappa_j'', |\kappa_j''| > \kappa_c), \qquad (22)$$

so that the SGS flux is carried by $c^s$ and $u_3^s$ modes whose wavenumbers are beyond the cutoff but whose difference wavenumber falls within the cutoff.

Since at heights $z$ much smaller than the scale of the spatial filter (i.e., $z/\Delta \ll 1$) the SGS flux $\tilde{F}_3^r(z) \approx (c^s u_3^s)^r$ is a good surrogate for $\tilde{F}_0^r$, we can form a conservation equation for $\tilde{F}_0^r$:

$$\frac{\partial \tilde{F}_0^r}{\partial t} \approx \frac{\partial (c^s u_3^s)^r}{\partial t} = \left(c^s \frac{\partial u_3^s}{\partial t}\right)^r + \left(u_3^s \frac{\partial c^s}{\partial t}\right)^r, \qquad z/\Delta \ll 1. \qquad (23)$$

The $u_i^s$ and $c^s$ equations are derived by high-pass filtering (10) and (11). Carrying out the operations in (23) and simplifying as discussed in appendix A yields the resolvable-scale surface flux conservation equation, or budget:

$$\begin{aligned}
\frac{\partial}{\partial t}\tilde{F}_0^r \approx\ & -((u_{3,j}^r u_j^r)^s c^s)^r && \text{resolvable shear, cross flux interaction} && \text{(RSCFI)}\\
& -((c_{,j}^r u_j^r)^s u_3^s)^r && \text{resolvable gradient, cross stress interaction} && \text{(RGCSI)}\\
& -(u_{3,j}^r (u_j^s c^s)^r)^r && \text{resolvable-scale shear production} && \text{(RSSP)}\\
& -(u_j^r \tilde{F}_3^r)_{,j}^r && \text{large-scale advection} && \text{(LSA)}\\
& -U_j \tilde{F}_{0,j}^r && \text{mean advection} && \text{(MA)}\\
& -(u_j^s u_3^s c^s)_{,j}^r && \text{small-scale advection} && \text{(SSA)}\\
& -(c_{,j}^r (u_j^s u_3^s)^r)^r && \text{resolvable-scale gradient production} && \text{(RSGP)}\\
& -C_{,3}(u_3^s u_3^s)^r && \text{mean gradient production} && \text{(MGP)}
\end{aligned}$$

$$+\ \frac{g}{T_0}(\theta^s c^s)^r \qquad \text{buoyant production} \qquad \text{(BP)}$$
$$-\ (p^s_{,3} c^s)^r \qquad \text{pressure destruction} \qquad \text{(PD).} \qquad (24)$$

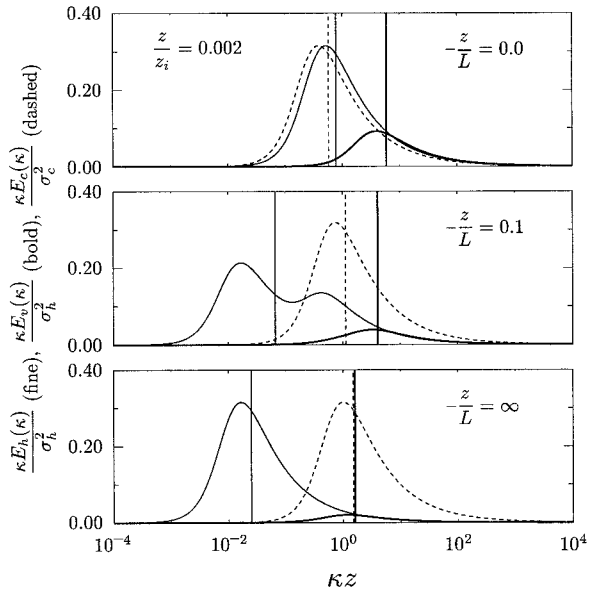


FIG. 3. The two-dimensional, surface-layer spectra of a scalar (dashed line), vertical velocity (bold line), and horizontal velocity (fine line), as modeled by Peltier et al. (1996). The vertical lines indicate the $\kappa z$ value below which lies 50% of the variance. Top: neutral; center: sightly unstable; bottom: free convection.

Let us relate Eq. (24) to the more familiar budget of the Reynolds flux $\overline{cu_3}$, where the overbar denotes the ensemble mean. Consider a horizontally homogeneous flow and let $\kappa_c \to 0$. In this limit each filtered field has only a $\kappa = 0$ component, the horizontal mean value, which because of the homogeneity is equal to the ensemble mean. Thus, $u_i^r \to 0$, $c^r \to 0$, and our decomposition (15) and (16) reduces to

$$\tilde{u}_i = U_i + u_i^s, \qquad \tilde{c} = C + c^s,$$
$$\tilde{\theta} = \Theta + \theta^s, \qquad \tilde{p} = P + p^s. \qquad (25)$$

It follows that

$$\text{as } \kappa_c \to 0,\ u_i^s \to u_i,\ c^s \to c,$$
$$\theta^s \to \theta,\ p^s \to p. \qquad (26)$$

In this limit the first through fifth and the seventh terms on the right side of the SGS flux budget (24) vanish. Thus, as $\kappa_c \to 0$ the SGS flux budget becomes, under horizontally homogeneous conditions,

$$\frac{\partial}{\partial t}\overline{u_3 c} = -(\overline{u_3 u_3 c})_{,3} - C_{,3}\overline{u_3 u_3} + \frac{g}{T_0}\overline{\theta c} - \overline{p_{,3} c}. \qquad (27)$$

This is the budget of the vertical component of the Reynolds scalar flux (Wyngaard et al. 1971).

We need to scale the terms in the resolvable-scale surface flux conservation equation (24) so that we can drop the smallest ones. Monin–Obukhov similarity (Panofsky and Dutton 1984) provides expressions for the variances of velocity and scalar fluctuations in the surface layer, but here we need to know also how the partitioning of these variances between resolvable and subgrid-scale contributions,

$$\overline{f^2} = \overline{(f^r)^2} + \overline{(f^s)^2}, \qquad (28)$$

depends on distance from the surface and the cutoff wavenumber of the filter. We develop these scaling relations next.

## 4. Scaling LES fields in the surface layer

Consider a zero-mean random variable $f = f^r + f^s$ (a fluctuating velocity component or scalar) in the surface layer. With wave-cutoff filtering we have

$$\overline{f^2} = \int_0^\infty E(\kappa)\, d\kappa = \int_0^{\kappa_c} E(\kappa)\, d\kappa + \int_{\kappa_c}^\infty E(\kappa)\, d\kappa$$
$$= \overline{(f^r)^2} + \overline{(f^s)^2}. \qquad (29)$$

For horizontal (subscript $h$) gradients we have

$$\overline{\left(\frac{\partial f^r}{\partial x_h}\right)^2} \sim \int_0^{\kappa_c} \kappa^2 E(\kappa)\, d\kappa, \qquad h = 1, 2. \qquad (30)$$

We will use (29) to determine how the variances of $u_h$, $c$, and $u_3$ for $z/\Delta \sim \kappa_c z \ll 1$ are partitioned into their resolvable and SGS parts. We will use (30) to determine how the variances of $u^r_{h,h}$, $u^r_{3,h}$, and $c^r_{,h}$ depend on $z$ and $\Delta$ for $z/\Delta \ll 1$.

### a. Horizontal velocity and scalars

For horizontal velocity and scalars the Peltier et al. (1996) model for $E(\kappa)$ given in Eq. (19) yields

$$\overline{(f^r)^2} = \frac{c_1 s^2}{c_2^{4/3}} \int_0^{\kappa_c l} \frac{\kappa l}{\left(1 + \frac{(\kappa l)^2}{c_2}\right)^{4/3}}\, d(\kappa l),$$

$$\overline{\left(\frac{\partial f^r}{\partial x_h}\right)^2} = \frac{c_1 s^2}{l^2 c_2^{4/3}} \int_0^{\kappa_c l} \frac{(\kappa l)^3}{\left(1 + \frac{(\kappa l)^2}{c_2}\right)^{4/3}}\, d(\kappa l). \qquad (31)$$

Under neutral conditions Peltier et al. chose $l = z$,

which makes $(\kappa l)^2/c_2$ a small parameter in (31), and we find

$$\overline{(f^r)^2} \approx \frac{c_1 s^2 (\kappa_c l)^2}{2c_2^{4/3}}, \qquad \overline{\left(\frac{\partial f^r}{\partial x_h}\right)^2} \approx \frac{c_1 s^2 (\kappa_c l)^4}{4l^2 c_2^{4/3}}. \quad (32)$$

For horizontal velocity and scalars these imply

neutral:

$$u_h^r \sim u_* \frac{z}{\Delta}, \qquad c^r \sim C_* \frac{z}{\Delta}, \qquad u_h^s \sim u_* \left[1 - \left(\frac{z}{\Delta}\right)^2\right],$$
$$c^s \sim C_* \left[1 - \left(\frac{z}{\Delta}\right)^2\right];$$
$$u_{h,h}^r \sim \frac{u_*}{\Delta}\left(\frac{z}{\Delta}\right), \qquad c_{,h}^r \sim \frac{C_*}{\Delta}\left(\frac{z}{\Delta}\right). \quad (33)$$

In free convection Peltier et al. chose $l = z_i$. For horizontal velocity $(\kappa_c l)^2/c_2$ is then a large parameter. Equation (31) yields in that limit

$$\overline{(f^r)^2} \approx \frac{3c_1 s^2}{2c_2^{1/3}}\left(1 - \frac{c_2^{2/3}}{(\kappa_c l)^{2/3}}\right), \qquad \overline{\left(\frac{\partial f^r}{\partial x_h}\right)^2} \approx \frac{3c_1 s^2 \kappa_c^{4/3}}{4l^{2/3}}, \quad (34)$$

which implies

free convection:

$$u_h^r \sim w_* \left[1 - \left(\frac{\Delta}{z_i}\right)^{2/3}\right],$$
$$u_h^s \sim w_* \left(\frac{\Delta}{z_i}\right)^{1/3} \sim u_f \left(\frac{z}{\Delta}\right)^{-1/3}, \qquad u_{h,h}^r \sim \frac{u_f}{\Delta}\left(\frac{z}{\Delta}\right)^{-1/3}. \quad (35)$$

For a scalar in free convection Peltier et al. found that $c_2 \sim (z_i/z)^2$, making $(\kappa l)^2/c_2$ a small parameter in (31) so that (32) applies. They found that $c_1 \sim (z_i/z)^{2/3}$, so that

free convection:

$$c^r \sim C_f \frac{z}{\Delta}, \qquad c^s \sim C_f \left[1 - \left(\frac{z}{\Delta}\right)^2\right],$$
$$c_{,h}^r \sim \frac{C_f}{\Delta}\left(\frac{z}{\Delta}\right). \quad (36)$$

### b. Vertical velocity

Peltier et al. used a slightly different model for the two-dimensional spectrum $E_v$ of vertical velocity $u_3$ in the surface layer:

$$E_v(\kappa) = T(\kappa) E(\kappa). \quad (37)$$

$T(\kappa)$ is a ''continuity transfer function,''

$$T(\kappa) = \frac{(\kappa z)^2}{0.62 + \frac{7}{8}(\kappa z)^2}, \quad (38)$$

that models the influence of the surface at $\kappa z \ll 1$ and ensures that $E_v$ behaves as required by local isotropy at $\kappa z \gg 1$.

Under neutral conditions $l = z$ so that $\kappa_c z \ll 1$. In this limit we can simplify (37) to

$$E_v(\kappa) \sim 1.6(\kappa z)^2 E(\kappa) \quad (39)$$

so that the variance expressions are

$$\overline{(f^r)^2} \approx \frac{1.6 c_1 s^2}{c_2^{4/3}} \int_0^{\kappa_c z} \frac{(\kappa z)^3}{(1 + (\kappa z)^2/c_2)^{4/3}}\, d(\kappa z),$$
$$\overline{\left(\frac{\partial f^r}{\partial x_h}\right)^2} \approx \frac{1.6 c_1 s^2}{z^2 c_2^{4/3}} \int_0^{\kappa_c z} \frac{(\kappa z)^5}{(1 + (\kappa z)^2/c_2)^{4/3}}\, d(\kappa z). \quad (40)$$

These imply

neutral:

$$u_3^r \sim u_* \left(\frac{z}{\Delta}\right)^2, \qquad u_3^s \sim u_* \left[1 - \left(\frac{z}{\Delta}\right)^4\right],$$
$$u_{3,h}^r \sim \frac{u_*}{\Delta}\left(\frac{z}{\Delta}\right)^2. \quad (41)$$

Under free convection $l = z_i$ and the expressions are

$$\overline{(f^r)^2} \approx \frac{1.6 c_1 s^2}{c_2^{4/3}} \int_0^{\kappa_c z_i} \frac{(\kappa z)^2 (\kappa z_i)}{(1 + (\kappa z_i)^2/c_2)^{4/3}}\, d(\kappa z_i),$$
$$\overline{\left(\frac{\partial f^r}{\partial x_h}\right)^2} \approx \frac{1.6 c_1 s^2}{z_i^2 c_2^{4/3}} \int_0^{\kappa_c z_i} \frac{(\kappa z)^2 (\kappa z_i)^3}{(1 + (\kappa z_i)^2/c_2)^{4/3}}\, d(\kappa z_i). \quad (42)$$

Here, $\kappa_c z_i$ is a large parameter and we have

free convection:

$$u_3^r \sim u_f \left(\frac{z}{\Delta}\right)^{2/3}, \qquad u_3^s \sim u_f \left[1 - \left(\frac{z}{\Delta}\right)^{4/3}\right];$$
$$u_{3,h}^r \sim \frac{u_f}{\Delta}\left(\frac{z}{\Delta}\right)^{2/3}. \quad (43)$$

### c. Vertical gradients

The vertical inhomogeneity of the surface layer makes rms vertical gradients more difficult to estimate. For resolvable-scale variables this inhomogeneity can take two forms: a $z$-dependence of amplitude and a $z$-dependence of vertical spatial scale. We separate these two inhomogeneities by writing a zero-mean, resolvable-scale variable $f^r$ as

$$f^r(x_i, t) = A(x_3) s(x_i, t). \quad (44)$$

Here $A$ is a nonrandom scaling function that contains

the vertical inhomogeneity in amplitude. The function $s$ is random, with zero mean and unit variance; it contains whatever vertical inhomogeneity in vertical spatial scale exists in $f^r$. It is possible that the vertical spatial scales of $u_3^r$ vary with $z$, for example. Since $s$ has unit variance, it follows from (44) that $\overline{(f^r)^2} = A^2$. In the case of $u_3^r$ under neutral conditions, for example, (41) implies that $A \sim u_*(z/\Delta)^2$.

Differentiating (44) with respect to $x_3$, squaring, and averaging gives

$$\overline{(f^r_{,3})^2} = A^2\overline{(s_{,3})^2} + (\overline{s^2})_{,3}A_{,3}A + (A_{,3})^2 = A^2\overline{(s_{,3})^2} + (A_{,3})^2, \quad (45)$$

the cross term vanishing because we chose $\overline{s^2}$ to be independent of $z$. The gradient variances $\overline{(s_{,h})^2}$ and $\overline{(s_{,3})^2}$ are related to $\overline{s^2}$ through the Taylor microscales $\lambda_h$ and $\lambda_z$ (Tennekes and Lumley 1972):

$$\lambda_h^2 = \overline{s^2}/\overline{(s_{,h})^2}, \qquad \lambda_z^2 = \overline{s^2}/\overline{(s_{,3})^2}. \quad (46)$$

With (46) we can write (45) as

$$\overline{(f^r_{,3})^2} = A^2\frac{\lambda_h^2}{\lambda_z^2}\overline{(s_{,h})^2} + (A_{,3})^2. \quad (47)$$

Differentiating (44) with respect to $x_h$, squaring, averaging, and combining with (47) yields

$$\overline{(f^r_{,3})^2} = \frac{\lambda_h^2}{\lambda_z^2}\overline{(f^r_{,h})^2} + (A_{,3})^2. \quad (48)$$

Our results in sections 4a and 4b show that for most of the resolvable-scale variables the horizontal Taylor microscale $\lambda_h$ is $\Delta$, the smallest surviving horizontal scale in the filtered fields. We will assume that $\lambda_z$ is of this order as well so that (48) becomes

$$\overline{(f^r_{,3})^2} = \overline{(f^r_{,h})^2} + (A_{,3})^2. \quad (49)$$

Let us illustrate with $u_3^r$ under neutral conditions. Equation (49) yields

$$\overline{(u^r_{3,3})^2} \sim \frac{u_*^2}{\Delta^2}\left(\frac{z}{\Delta}\right)^4 + \frac{u_*^2}{\Delta^2}\left(\frac{z}{\Delta}\right)^2. \quad (50)$$

The second term on the right dominates at small $z/\Delta$ so that our assumption that $\lambda_z \sim \lambda_h \sim \Delta$ is not critical; we obtain the result (50) for $\lambda_z \sim z$ as well. This is the case for almost all variables.

This procedure yields the scaling estimates

neutral:

$$u^r_{3,3} \sim \frac{u_*}{\Delta}\left(\frac{z}{\Delta}\right), \qquad c^r_{,3} \sim \frac{C_*}{\Delta}, \qquad u^r_{h,3} \sim \frac{u_*}{\Delta};$$

free convection:

$$u^r_{3,3} \sim \frac{u_f}{\Delta}\left(\frac{z}{\Delta}\right)^{-1/3}, \qquad c^r_{,3} \sim \frac{C_f}{\Delta}, \qquad u^r_{h,3} \sim \frac{u_f}{\Delta}\left(\frac{z}{\Delta}\right)^{-1/3}. \quad (51)$$

From (33), (35), and (51) we see that $u^r_{1,1}$, $u^r_{2,2}$, and $u^r_{3,3}$ are of the same order, consistent with the resolvable-scale continuity equation.

## 5. Simplifying the resolvable-scale surface-flux budget

### a. The ''constant-SGS-flux'' layer

We can use our surface-layer scaling relations of section 4 to quantify the variation of SGS flux with height near the surface. We first decompose the SGS flux into ensemble-mean and fluctuating parts,

$$\tilde{F}^r_3 = F_0 + f_3. \quad (52)$$

We assume that the two flux-divergence terms in the resolvable-scale scalar conservation equation (14) are of the same order:

$$\tilde{F}^r_{3,3} \sim \tilde{F}^r_{j,j} \sim (\tilde{c}^r_{,j}\tilde{u}^r_j)^r. \quad (53)$$

Our scaling estimates in section 4 then imply

$$\tilde{F}^r_{3,3} \sim \frac{F_0}{\Delta}\left(\frac{z}{\Delta}\right)^2 \quad \text{(neutral)},$$

$$\frac{F_0}{\Delta}\left(\frac{z}{\Delta}\right)^{2/3}\left(\frac{z_i}{\Delta}\right)^{1/3} \quad \text{(free convection)}. \quad (54)$$

This says that the SGS flux divergence vanishes as $z/\Delta \to 0$ because the forcing terms in the resolvable-scale scalar equation vanish in that limit.

Equation (54) implies that the rms difference between the resolvable-scale surface flux $\tilde{F}^r_0$ and the SGS flux at height $z$, $\tilde{F}^r_3(z)$, scaled by the mean surface flux $F_0$, is of order

$$\frac{\tilde{F}_0 - \tilde{F}^r_3(z)}{F_0} \sim \frac{z\tilde{F}^r_{3,3}}{F_0} \sim \left(\frac{z}{\Delta}\right)^3 \quad \text{(neutral)},$$

$$\left(\frac{z}{\Delta}\right)^{5/3}\left(\frac{z_i}{\Delta}\right)^{1/3} \quad \text{(free convection)}. \quad (55)$$

Let us compare this rms flux difference to the rms fluctuations in SGS flux at height $z \ll \Delta$. Estimating the rms value of the fluctuating SGS flux $F'_3$ from the usual surface-exchange formulation gives

$$\frac{F'_3}{F_0} \sim \frac{\sigma_u}{U_1}, \quad (56)$$

where $\sigma_u$ is the rms fluctuation in the streamwise wind, typically in the range $(0.1–0.5)U_1$.

We conclude that at small $z/\Delta$, the rms difference in SGS flux between the surface and height $z$, Eq. (55), is small compared to the rms fluctuation level in SGS flux at height $z$, Eq. (56). If so, when $z/\Delta \ll 1$ the SGS flux at $z$ is a reliable surrogate for the resolvable-scale surface flux.

It remains to evaluate the importance of the cross contributions to the SGS scalar flux, Eq. (17). In ap-

pendix B we show their rms values are of the order of $F_0\,(z/\Delta)^3$. Thus, at height $z \ll \Delta$ they are not larger than the rms difference in SGS flux between the surface and height $z$. Since we judged the latter to be negligible, we will continue to neglect the cross contributions to SGS flux as well.

### b. Scaling the flux budget

We can now scale some of the terms in the resolvable-scale surface flux budget (24). We choose the $x_1$ direction to be that of the mean wind so that $U_i = (U_1, 0, 0)$. The scaling results are summarized in Table 1. We cannot directly scale pressure destruction, but from experience with the Reynolds flux budget close to the surface (Wyngaard et al. 1971) we expect that it is a leading term.

To scale the time-change term, not included in Table 1, we assume that the local rate of change of the resolvable-scale surface flux is determined by resolvable-scale processes. Thus, we take the time-change term to be of the order of mean advection at neutral and large-scale horizontal advection in free convection, giving

$$\frac{\partial \tilde{F}_0^r}{\partial t} \sim F_0 \frac{u_*}{z}\left(\frac{z}{\Delta}\right)^2 \qquad \text{(neutral)},$$

$$\sim F_0 \frac{u_f}{z}\left(\frac{z}{\Delta}\right)^{2/3}\left(\frac{z_i}{\Delta}\right)^{1/3} \qquad \text{(free convection)}. \tag{57}$$

### c. A hierarchy of resolvable-scale surface-flux budgets

According to the scaling results of Table 1 the budget of surface scalar flux takes different forms depending on the value of $z_1/\Delta$.

#### 1) $z_1/\Delta \ll 1$

When $z/\Delta \ll 1$ we need retain only the $O(1)$ terms in the resolvable-scale surface-flux conservation equation (24), and it reduces to

$$0 \approx -(u_3^s u_3^s c^s)^r_{,3} - C_{,3}(u_3^s u_3^s)^r + \frac{g}{T_0}(\theta^s c^s)^r - (p^s_{,3} c^s)^r. \tag{58}$$

The $\kappa = 0$ mode of Eq. (58), its expected value, is the quasi-steady form of Eq. (27), the locally homogeneous Reynolds budget of scalar flux. The terms in Eqs. (58) and (27) represent, in order, the rates of vertical transport of turbulent flux by small-scale turbulence, production through the interaction of vertical velocity fluctuations with the mean vertical gradient of the quantity being transported, production through buoyancy, and destruction by pressure gradient interactions.

In the locally homogeneous, quasi-steady surface layer, there exists well-established flux-gradient and surface-exchange relations (Businger et al. 1971):

TABLE 1. Scaling of terms in the budget of surface scalar flux.

| | |
|---|---|
| RSCFI: | $((u^r_{3,j}u^r_j)^s c^s)^r \sim u^r_{3,j}u^r_j \delta c_s \sim u^r_{3,j}u^r_j c^r$ |
| RGCSI: | $((c^r_{,j}u^r_j)^s u^s_3)^r \sim c^r_{,j}u^r_j \delta u^s_3 \sim c^r_j u^r_j u^r_3$ |
| RSSP: | $(u^r_{3,j}(u^s_j c^s)^r)^r \sim u^r_{3,j}u^s_j c^s$ |
| LSA: | $(u^r_j \tilde{F}^r_3)^r_{,j} \sim u^r_j \tilde{F}^r_{3,j} \sim \frac{u^r_h F_0 u^r_{h,h}}{U_1}, \quad j = 1, 2;$ |
| | $\sim u^r_3(c^r_{,h}u^r_h + c^r_{,3}u^r_3), \quad j = 3$ |
| MA: | $U_j \tilde{F}^r_{0,j} \sim u^r_{h,h}F_0$ |
| SSA: | $(u^s_j u^s_3 c^s)^r_{,j} \sim (u^s_j u^s_3 c^s)_{,j}$ |
| RSGP: | $(c^r_{,j}(u^s_j u^s_3)^r)^r \sim c^r_{,j}u^s_j u^s_3$ |
| MGP: | $C_{,3}(u^s_3 u^s_3)^r \sim C_{,3}u^s_3 u^s_3$ |
| BP: | $\frac{g}{T_0}(\theta^s c^s)^r \sim \frac{g}{T_0}\theta^s c^s$ |
| PD: | $(p^s_{,3}c^s)^r \sim p^s_{,3}c^s$ |

Mean surface flux $F_0 = u_* C_* = u_f C_f$

| | Neutral (units of $F_0 \frac{u_*}{z}$) | | Free convection (units of $F_0 \frac{u_f}{z}$) | |
|---|---|---|---|---|
| Term | $j = 1, 2$ | $j = 3$ | $j = 1, 2$ | $j = 3$ |
| RSCFI | $\left(\frac{z}{\Delta}\right)^5$ | $\left(\frac{z}{\Delta}\right)^5$ | $\left(\frac{z}{\Delta}\right)^{7/3}\left(\frac{z_i}{\Delta}\right)^{1/3}$ | $\left(\frac{z}{\Delta}\right)^{7/3}$ |
| RGCSI | $\left(\frac{z}{\Delta}\right)^5$ | $\left(\frac{z}{\Delta}\right)^5$ | $\left(\frac{z}{\Delta}\right)^{7/3}\left(\frac{z_i}{\Delta}\right)^{1/3}$ | $\left(\frac{z}{\Delta}\right)^{7/3}$ |
| RSSP | $\left(\frac{z}{\Delta}\right)^3$ | $\left(\frac{z}{\Delta}\right)^2$ | $\left(\frac{z}{\Delta}\right)^{4/3}$ | $\left(\frac{z}{\Delta}\right)^{2/3}$ |
| LSA | $\left(\frac{z}{\Delta}\right)^3\left(\frac{u_*}{U_1}\right)$ | $\left(\frac{z}{\Delta}\right)^5$ | $\left(\frac{z}{\Delta}\right)^{2/3}\left(\frac{z_i}{\Delta}\right)^{1/3}$ | $\left(\frac{z}{\Delta}\right)^{7/3}\left(\frac{z_i}{\Delta}\right)^{1/3}$ |
| MA | $\left(\frac{z}{\Delta}\right)^2$ | 0 | 0 | 0 |
| SSA | $\left(\frac{z}{\Delta}\right)$ | 1 | $\left(\frac{z}{\Delta}\right)$ | 1 |
| RSGP | $\left(\frac{z}{\Delta}\right)^2$ | $\left(\frac{z}{\Delta}\right)$ | $\left(\frac{z}{\Delta}\right)^2$ | $\left(\frac{z}{\Delta}\right)$ |
| MGP | 1 | | 1 | |
| BP | 0 | | 1 | |
| PD | 1 | | 1 | |

$$\overline{wc} = -KC_{,3}; \qquad F_0 = C_H(z)U_1(z)[C(z_{0c} - C(z)] = C_H(z)U_1(z)\Delta C(z). \tag{59}$$

Here $z_{0c}$ is the ''roughness length'' for the scalar. In (59) we have shown explicitly only the dependence on $z$. The dependence on stability is represented well through the Monin–Obukhov similarity hypothesis (Panofsky and Dutton 1984).

The turbulence active in the processes represented in

(58) is subgrid scale; it has a dominant length scale $z$ and timescales $T_s \sim z/u_*$ and $z/u_f$ in the neutral and free-convection limits, respectively. The final filtering of each term can be thought of roughly as averaging over horizontal spatial scales $\Delta \gg z$. The time-change term is negligible because its timescale is much greater than $T_s$. Similarly, the horizontal inhomogeneity of filtered variables is weak because it occurs on a spatial scale much larger than $z$. Thus, we argue that for $z/\Delta \ll 1$ the resolvable-scale surface flux budget (58) represents a quasi-steady, locally homogeneous state of ''local grid-volume equilibrium.''

The analogy between the Reynolds flux budget (27) and the $z/\Delta \to 0$ limit of the resolvable-scale surface-flux budget (58), the well-behaved surface-exchange relation (59) for the Reynolds flux, and the ''coupling eddies'' notion of Fig. 1 make it plausible that in this limit the resolvable-scale surface flux displays a surface-exchange relation like (59), but with resolvable-scale variables replacing the ensemble averages:

$$\tilde{F}_0^r(x_1, x_2, t) = C_H(z/\tilde{L})[\tilde{u}_1^r(x_1, x_2, z, t)\Delta\tilde{c}^r(x_1, x_2, z, t)]^r, \quad z/\Delta \ll 1. \tag{60}$$

Here $C_H$ is the mean surface-exchange coefficient that depends on stability; here the stability is interpreted locally, however. For that purpose we define the local stability parameter for the grid volume, $z_1/\tilde{L}$, with $\tilde{L}$ the local Monin–Obukhov length,

$$\tilde{L} = -\frac{\tilde{u}_*^3 T_0}{kg\tilde{Q}_0}, \tag{61}$$

and $\tilde{u}_*$ and $\tilde{Q}_0$ the local SGS friction velocity and surface temperature flux. Based on Eq. (58) we would expect $\Delta C$ rather than $\Delta\tilde{c}^r$ to appear in (60), but section 4 indicates that this difference is negligible for $z/\Delta \ll 1$ and (60) is consistent with typical practice in LES.

### 2) $z_1/\Delta$ SMALL BUT NOT NEGLIGIBLE

Table 1 shows that in free convection the horizontal part of large-scale advection (LSA) is significant at $z_1$ such that

$$\left(\frac{z_1}{\Delta}\right)^{2/3}\left(\frac{z_i}{\Delta}\right)^{1/3} \sim 1, \quad \text{or} \quad z_1 \sim \frac{\Delta^{3/2}}{z_i^{1/2}}. \tag{62}$$

For $\Delta = 10$ m and $z_i = 10^3$ m this occurs at $z_1 = 1$ m. The same arguments hold for the time-change term, Eq. (24). We conclude that in application to fine-mesh LES with $z_1$ on the order of a few meters, the time-change and horizontal LSA terms in the surface-flux budget (24) can be significant.

If we combine the LSA and MA terms by writing $U_1 + u_h^r = \tilde{u}_h^r$, as we previously did with the RSGP and MGP terms, Eq. (24) becomes

$$\frac{\partial}{\partial t}\tilde{F}_0^r + (\tilde{u}_i^r\tilde{F}_0^r)_{,i}^r + (u_3^s u_3^s c^s)_{,3}^r + \tilde{c}_{,3}^r(u_3^s u_3^s)^r - \frac{g}{T_0}(\theta^s c^s)^r \approx -(p_{,3}^s c^s)^r, \tag{63}$$

where the index $i$ is summed over 1 and 2. Equation (63) represents a departure from the local-grid-volume-equilibrium state of Eq. (58) in that it includes horizontal advection and time change of resolvable-scale surface flux in addition to the production, small-scale advection, and pressure-destruction processes.

Let us model the local time-change and horizontal advection effects through a hypothesis advanced by Bradshaw (1969) and discussed by Wyngaard (1982). We assume that the SGS turbulence remains in local grid volume equilibrium in the sense that

$$(u_3^s u_3^s c^s)_{,3}^r + (\tilde{c}_{,3}^r)_{\text{eq}}(u_3^s u_3^s)^r - \frac{g}{T_0}(\theta^s c^s)^r = -(p_{,3}^s c^s)^r, \tag{64}$$

where $(\tilde{c}_{,3}^r)_{\text{eq}}$ is the local-grid-volume-equilibrium value of the resolvable-scale scalar gradient in the vertical. Because $z_1/\Delta$ is small, there are many coupling eddies in the grid volume and to first approximation we can take $(\tilde{c}_{,3}^r)_{\text{eq}}$ to be nonrandom and to have a similarity form identical to that of the traditional M–O function for temperature, $\phi_h$:

$$(\tilde{c}_{,3}^r)_{\text{eq}} = -\frac{\tilde{F}_0^r}{k\tilde{u}_* z_1}\phi_h(z_1/\tilde{L}), \qquad \phi_h = -\frac{kzu_*}{Q_0}\frac{\partial\Theta}{\partial z}. \tag{65}$$

Using (64) in (63) yields

$$\frac{\partial}{\partial t}\tilde{F}_0^r + (\tilde{u}_h^r\tilde{F}_0^r)_{,h}^r \simeq (u_3^s u_3^s)^r((\tilde{c}_{,3}^r)_{\text{eq}} - \tilde{c}_{,3}^r). \tag{66}$$

In order to solve Eq. (66) the local value of the SGS vertical velocity variance $(u_3^s u_3^s)^r$ is needed; it could be obtained through a local similarity model

$$(u_3^s u_3^s)^r = \tilde{u}_*^2 f(z_1/\tilde{L}), \tag{67}$$

where $f$ is the M–O function for vertical velocity variance. With such a model for $(u_3^s u_3^s)^r$, Eq. (66) indicates how the scalar gradient differs from the local-grid-volume-equilibrium value if there is local time change or horizontal advection of resolvable-scale surface flux.

If we approximate (66) by

$$\frac{\partial}{\partial t}\tilde{F}_0^r + (\tilde{u}_h^r\tilde{F}_0^r)_{,h}^r \approx \frac{(u_3^s u_3^s)^r}{z_1}(\Delta\tilde{c}^r - \Delta\tilde{c}_{\text{eq}}^r) \tag{68}$$

and introduce the mean and local surface-exchange coefficients,

$$(\Delta\tilde{c}^r)_{\text{eq}} = \frac{\tilde{F}_0^r}{C_H\tilde{u}_1^r}, \qquad (\Delta\tilde{c}^r) = \frac{\tilde{F}_0^r}{\tilde{C}_H\tilde{u}_1^r}, \tag{69}$$

combining (68) and (69) then gives

$$\frac{\partial}{\partial t}\tilde{F}_0^r + (\tilde{u}_h^r\tilde{F}_0^r)_{,h}^r + \left(\frac{(u_3^s u_3^s)^r\tilde{F}_0^r}{z_1\tilde{u}_1^r}\right)\left(\frac{1}{C_H} - \frac{1}{\tilde{C}_H}\right) = 0. \tag{70}$$

This determines the departure of the local surface-exchange coefficient $\tilde{C}_H$ from its mean value $C_H$ due to the effects of local time change and horizontal advection of SGS flux.

3) $z_1/\Delta \leq 1$

In order to evaluate other candidate terms in the resolvable-scale surface flux budget, let us write (24) symbolically as

$$\frac{\partial \tilde{F}^r_0}{\partial t} = \sum_{i=1}^{n} T_i - \frac{\tilde{F}^r_0}{\tau}, \tag{71}$$

where the final term, a parameterization of the rate of pressure destruction, is patterned after its behavior in the Reynolds flux budget (Wyngaard et al. 1971), and $T_i$ represents the remaining terms. We estimate the rms contribution to $\tilde{F}^r_0$ from each component of $T_i$ as $\delta_i \tilde{F}^r_0 \sim \tau T_i$. As $z_1/\Delta \to 1$ these contributions increase since, according to Table 1, the $T_i$ increase. In fact, however, (24) describes the budget at $z_1$, not at the surface, and we showed in (55) that as $z_1/\Delta$ increases the rms difference between the fluxes at the surface and at height $z_1$ also increases. This suggests a criterion for retaining a term in (24): that its rms contribution to the flux be large compared to the rms difference between the resolvable-scale surface flux and the SGS flux at height $z_1$:

$$\delta_i \tilde{F}^r_0 \gg \tilde{F}^r_0 - \tilde{F}^r_3(z_1). \tag{72}$$

This ensures that the term does reflect a contribution primarily to the resolvable-scale surface flux.

Using our estimate (55) for $\tilde{F}^r_0 - \tilde{F}^r_3(z_1)$ and taking $\tau \sim z_1/u_*$ at neutral and $\tau \sim z_1/u_f$ in free convection then yields

$$T_i \left( \text{units of } F_0 \frac{u_*}{z_1} \right) \gg \left( \frac{z_1}{\Delta} \right)^3 \quad \text{(neutral)},$$

$$T_i \left( \text{units of } F_0 \frac{u_f}{z_1} \right) \gg \left( \frac{z_1}{\Delta} \right)^{5/3} \quad \text{(free convection)}. \tag{73}$$

Let us interpret "$\gg$" in (73) as meaning between one and two orders less in $z_1/\Delta$. We therefore also include the vertical part of RSSP. The surface flux budget then is

$$\frac{\partial}{\partial t}\tilde{F}^r_0 + (\tilde{u}^r_h \tilde{F}^r_0)^r_{,h} + (u^r_{3,3}\tilde{F}^r_0)^r + (u^s_3 u^s_3 c^s)^r_{,3} + [\tilde{c}^r_{,3}(u^s_3 u^s_3)^r]^r - \frac{g}{T_0}(\theta^s c^s)^r \approx -(p^s_{,3} c^s)^r. \tag{74}$$

Using the local-grid-volume-equilibrium hypothesis (64) for the SGS turbulence then gives an extension of (70):

$$\frac{\partial}{\partial t}\tilde{F}^r_0 + (\tilde{u}^r_h \tilde{F}^r_0)^r_{,h} + (u^r_{3,3}\tilde{F}^r_0)^r + \left( \frac{(u^s_3 u^s_3)^r \tilde{F}^r_0}{z_1 \tilde{u}^r_1} \right) \left( \frac{1}{C_H} - \frac{1}{\tilde{C}_H} \right) = 0. \tag{75}$$

Equation (75) further corrects the equilibrium surface-exchange expression for the production of resolvable-scale surface flux through the interaction of the SGS flux and the resolvable-scale velocity gradient $u^r_{3,3}$.

According to our scaling analysis in appendix B, the fractional contribution of the cross terms to the SGS flux is one to two orders smaller in $z/\Delta$ than the SGS flux fluctuations produced by the terms retained in (74). Thus, there seems no need to include the cross contributions to SGS flux.

### *d. Resolution in z*

Our scaling analysis of section 4 treats the effects of filtering the fields in the horizontal plane. Such filtering is done explicitly in Moeng's (1984) LES code, for example. Our analysis does not treat the effects of filtering or finite-difference approximations in $z$. Thus, our surface-layer scaling results are directly applicable only to LES with high vertical resolution.

The vertical resolution of LES also figures in the choice of a resolvable-scale surface flux model. The tradeoff is clear: if $z_1/\Delta \ll 1$, which requires the first grid point to be very close to the surface, a standard surface-exchange model for flux, Eq. (60), can be used. If $z_1/\Delta \approx 1$, the first grid point can be much higher but then more physics enters the resolvable-scale surface flux conservation equation, as indicated in Eq. (75). Thus, when $z_1/\Delta \ll 1$, the complicated connection between the resolvable-scale surface flux and the resolvable-scale flow at $z \sim \Delta$ must be made entirely through the SGS model; when $z_1/\Delta \approx 1$, some elements of that connection can be made through the resolvable-scale surface flux model.

## 6. Use of resolvable-scale surface-flux equations in LES

### *a. Implementation and results*

We implemented the $z_1/\Delta \leq 1$ form of the conservation equations for resolvable-scale surface temperature flux $\tilde{Q}^r_0$ and resolvable-scale surface stress $\tilde{\tau}^r_{0k}$ in Moeng's LES code (Moeng 1984). Using (69) for the surface-exchange coefficients, Eq. (75) can be rewritten for $\tilde{Q}^r_0$ as

$$\frac{\partial}{\partial t}\tilde{Q}^r_0 \approx -(\tilde{u}^r_h \tilde{Q}^r_0)^r_{,h} - (u^r_{3,3}\tilde{Q}^r_0)^r - [(u^s_3 u^s_3)^r(\tilde{\theta}^r_{,3} - (\tilde{\theta}^r_{,3})_{\text{eq}})]^r. \tag{76}$$

We used (65) for the local-grid-volume-equilibrium value of the resolvable-scale temperature gradient, where

$$\phi_h(z/\tilde{L}) = 0.74\left(1 - 9\frac{z}{\tilde{L}}\right)^{-1/2} \tag{77}$$

(Businger et al. 1971), $\tilde{L}$ is given by (61), and $\tilde{u}_*$ is given by

$$\tilde{u}_*^2 = \sqrt{(\tilde{\tau}^r_{01})^2 + (\tilde{\tau}^r_{02})^2}. \tag{78}$$

The local SGS vertical velocity variance is modeled as Eq. (67), where the nondimensional function is taken as

$$f(z/\tilde{L}) = 1.6 + 2.9\left(-\frac{z}{\tilde{L}}\right)^{2/3} \tag{79}$$

(Panofsky et al. 1977).

Our modeled conservation equation for the subgrid–subgrid part of the SGS stress, $(u^s_k u^s_3)^r = \tilde{S}^r_{0k}$, reduces to (appendix C)

$$\frac{\partial}{\partial t}\tilde{S}^r_{0k} \approx -(\tilde{u}^r_h \tilde{S}^r_{0k})^r_{,h} - (u^r_{3,3}\tilde{S}^r_{0k})^r - [(u^s_j u^s_3)^r(\tilde{u}^r_{k,j} - (\tilde{u}^r_{k,j})_{\text{eq}})]^r, \tag{80}$$

where $k = 1, 2$. The local-grid-volume-equilibrium value of the resolvable-scale velocity gradient is given by

$$(\tilde{u}^r_{k,j})_{\text{eq}} = -\frac{\tilde{\tau}_{0k}}{\tilde{u}_*^2}\frac{\tilde{u}_*}{kz_1}\phi_m(z_1/\tilde{L})\delta_{j3}, \tag{81}$$

where $\phi_m$ is taken as

$$\phi_m(z_1/\tilde{L}) = \left(1 - 15\frac{z}{\tilde{L}}\right)^{-1/4} \tag{82}$$

(Businger et al. 1971).

In section 2 of appendix C we show that the cross stress $\tilde{C}^r_{0k} = (u^r_k u^s_3 + u^s_k u^r_3)^r$ has zero mean but an rms value of order $u^r_k u^r_3$. We model it as

$$\tilde{C}^r_{0k} = u^r_k u'_3 + u'_k u^r_3, \tag{83}$$

where a prime denotes the rms value of the resolvable-scale field. The model (83) has zero mean, has an rms value of the required order, and depends on both the horizontal and vertical components of the resolved velocity.

Equations (76) and (80) were solved using a second-order, explicit Adams–Bashforth time marching scheme in which the temperature flux, for example, at time step $n + 1$ is given by

$$\tilde{Q}^r_0(n+1) = \tilde{Q}^r_0(n) + \Delta t\frac{3}{2}R_Q(n) - \Delta t\frac{1}{2}R_Q(n-1), \tag{84}$$

where $\Delta t$ is the time step, and $R_Q(n)$ is the right-hand side of (76) at time step $n$.

Since $z_1/\Delta$ is a critical parameter in our analysis, we carried out three sets of simulations: $64^3$, $128^2 \times 64$, and $192^2 \times 64$, with $z_1/\Delta$ of 0.13, 0.27, and 0.4, respectively, for a moderately convective boundary layer ($-z_i/L \approx 10$). Figure 2 shows the fluctuation levels in the surface-exchange coefficients obtained by using conservation equations for resolvable-scale surface fluxes in the simulations. These levels agree well with the findings of Wyngaard and Peltier (1996). The fluctuation levels in $\tilde{S}^r_{0k}$ and $\tilde{C}^r_{0k}$ are roughly of the same order.

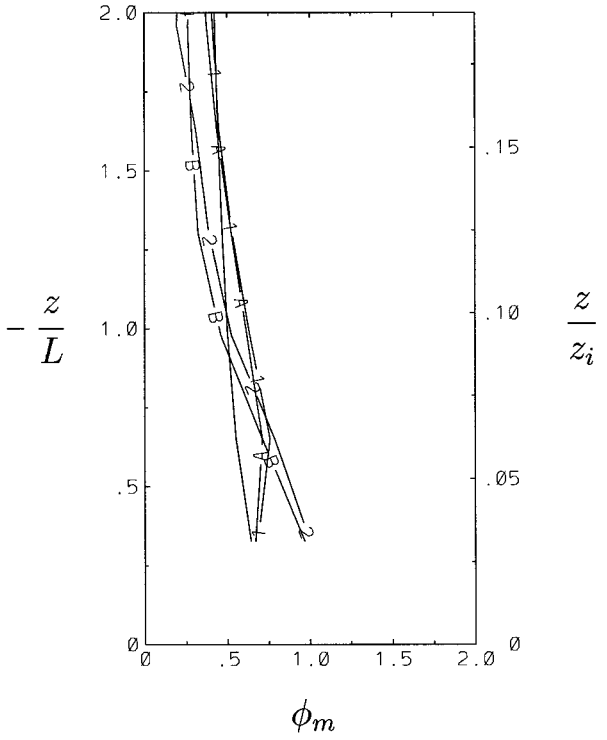


FIG. 4. Nondimensional mean shear in a moderately convective boundary layer ($-z_i/L \approx 10$). Curves 1 and 2 are from $64^3$ and $128^2 \times 64$ simulations, respectively, using surface-exchange coefficients; curves A and B are from $64^3$ and $128^2 \times 64$ simulations, respectively, using surface-flux equations; solid line is the empirical function of Businger et al. (1971)

Figures 4–6 show the nondimensional mean shear $\phi_m$, mean potential temperature gradient $\phi_h$, and vertical velocity variance, respectively, from $64^3$ and $128^2 \times 64$ simulations using the conservation equations (curves A and B) and the standard surface-exchange coefficients (curves 1 and 2). The profiles observed in past field experiments are also plotted in these figures.

Consistent with the experience of Mason and Thomson (1992) and Sullivan et al. (1994) $\phi_m$ is overpredicted, with respect to the observations, by the Smagorinsky-based SGS model (used in Moeng's code) with surface-exchange coefficients. Moreover, the profile kink moves closer to the surface as the horizontal resolution is increased.

In the $64^3$ simulation with surface-exchange coefficients, $\phi_h$ is somewhat lower than the measured value at the first grid point; above that it is slightly overpredicted. Increasing the horizontal resolution to $128^2$, while keeping the vertical resolution the same, limits

the overprediction of $\phi_h$ to the second grid point. The values at other grid points agree well with the field observations.

The nondimensional vertical-velocity variance in both the $64^3$ and the $128^2 \times 64$ simulations with surface-exchange coefficients are slightly lower than the field measurements reported by Panofsky et al. (1977). The change in resolution does not alter the profile significantly.

The use of flux-conservation equations instead of the surface-exchange coefficients yields slight improvements in all three profiles, most noticeably in that of vertical-velocity variance. However, the improvement is only marginal and not wholly satisfactory. We believe that the mild influence of improved lower boundary conditions on the mean surface-layer structure is due to deficiencies in the SGS model. The objective of surface-flux budgets is to capture more reliably the local structure of the resolvable-scale surface fluxes, but, as we show next, the Smagorinsky-based SGS model represents the surface-layer physics poorly and therefore presumably responds to enhanced structure in surface fluxes improperly as well.

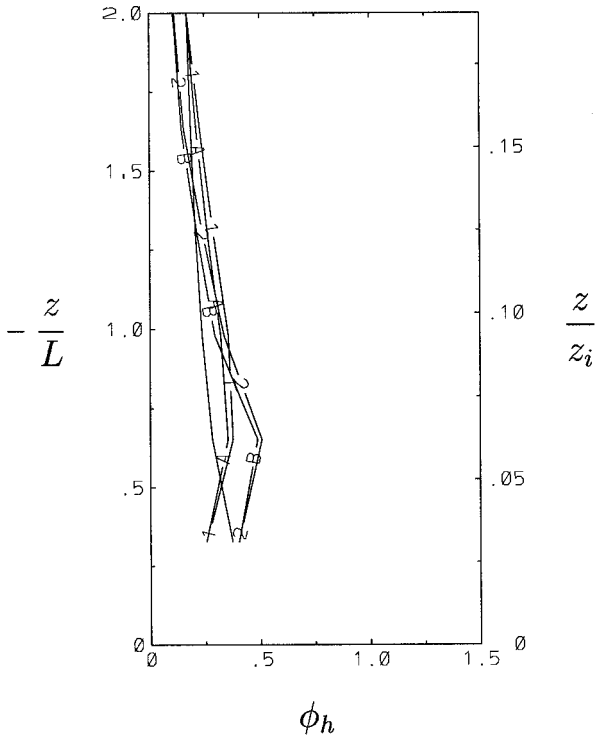


FIG. 5. Nondimensional mean temperature gradient in a moderately convective boundary layer ($-z_i/L \approx 10$). Curves 1 and 2 are from $64^3$ and $128^2 \times 64$ simulations, respectively, using surface-exchange coefficients; curves A and B are from $64^3$ and $128^2 \times 64$ simulations, respectively, using surface-flux equations; solid line is the empirical function of Businger et al. (1971).

### *b. Analysis of the SGS model from highly resolved surface-layer fields*

The Smagorinsky-type SGS model has been standard in LES since the early work of Lilly (1967) and Deardorff (1970). Its popularity stems from its simplicity and, most importantly, the insensitivity of resolved-scale fields to the SGS model in well-resolved turbulent flows. Near the surface, however, the vertical motions are always inadequately resolved and as a result the SGS closure becomes crucial there.

We analyzed the accuracy of Smagorinsky closure in the surface layer using highly resolved LES with nested meshes. Such tests have been done previously using direct numerical simulation (DNS) of isotropic turbulence (Clark et al. 1979; Bardina et al. 1983) and the neutral turbulent boundary layer (Piomelli et al. 1991). The unstable atmospheric surface layer, however, has certain distinct features not present in homogeneous turbulence and neutral boundary layers. Specifically, the horizontal motions in the surface layer of an unstable atmospheric boundary layer (ABL) are strongly influenced by the $z_i$-scaled mixed-layer eddies, causing a strong anisotropy of length and intensity scales between the horizontal and vertical motions. There is also a substantial horizontal mean temperature flux in the surface layer that is absent in the neutral boundary layer. Thus, past studies using DNS fields are not directly relevant for our analysis.

We generated highly resolved surface-layer fields using a three-level nested-mesh LES discussed in Khanna and Brasseur (1996). The full boundary layer was simulated at $-z_i/L \approx 10$ using a $128^3$ mesh covering a domain of $5z_i \times 5z_i \times 2z_i$. The next level of refinement in the surface layer was attained by an effective $256^3$ mesh covering a domain of $5z_i \times 5z_i \times 0.125z_i$, and the final level was attained by an effective $512^3$ mesh covering $5z_i \times 5z_i \times 0.06125z_i$ of the boundary layer. The upper boundary conditions for the embedded meshes were obtained from the next-level coarser domains with a one-way communication between the domains. At a height where the effective $512^3$ simulation resolved approximately 90% of the vertical fluxes and variances (the sixth grid level, at $z/z_i \approx 0.02$) the resolved variables were treated as fully resolved fields. They were decomposed into a resolvable part and a subgrid part by two-dimensional horizontal wave-cutoff filtering with a cutoff wavenumber corresponding to a $96^2$ horizontal mesh.

Table 2 compares the calculated SGS stresses and fluxes and their divergences with the values predicted by the SGS model used by Moeng (1984). The magnitudes of the cross-correlation coefficients of the modeled and actual SGS flux components are very low (less than 0.20). Those for SGS flux divergences, which appear in the dynamical equations, are particularly low (less than 0.05 for the horizontal components of the divergences). The SGS model also fails in capturing the mean diagonal SGS stress components, presumably due to its inability to reproduce the anisotropic distribution

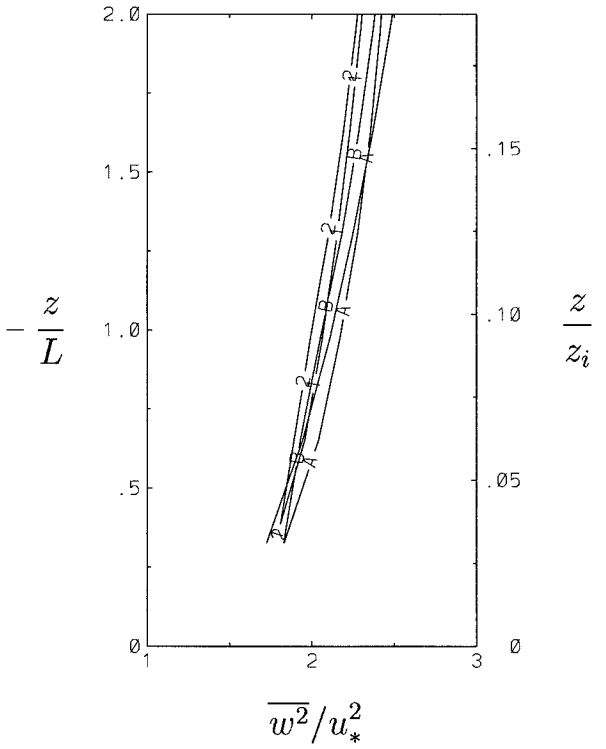


FIG. 6. Nondimensional vertical-velocity variance in a moderately convective boundary layer ($-z_i/L \approx 10$). Curves 1 and 2 are from $64^3$ and $128^2 \times 64$ simulations, respectively, using surface-exchange coefficients; curves A and B are from $64^3$ and $128^2 \times 64$ simulations, respectively, using surface-flux equations; solid line is the empirical function of Businger et al. (1971).

TABLE 2. A comparison of predicted and actual subgrid-scale temperature flux and stress components from an effective $512^3$ simulation, using nested meshes, of the atmospheric boundary layer ($-z_i/L \approx 8$). The comparisons are made at $z/z_i \approx 0.04$ and $z/\Delta \approx 0.75$; ($\tilde{q} = \tilde{F}_{i,i}$; $\tilde{a}_i = \tilde{\tau}_{ij,j}$).

| | Actual mean | Actual rms | Predicted/ actual (mean) | Predicted/ actual (rms) | Cross-correlation coefficient |
|---|---|---|---|---|---|
| | | | SGS flux | | |
| $\tilde{F}_1$ | −0.14 | 0.62 | 0.01 | 0.17 | 0.19 |
| $\tilde{F}_2$ | — | 0.45 | — | 0.33 | 0.25 |
| $\tilde{F}_3$ | 0.16 | 0.47 | 0.94 | 0.50 | 0.26 |
| $\tilde{F}_{1,1}$ | — | 0.43 | — | 0.22 | 0.21 |
| $\tilde{F}_{2,2}$ | — | 0.42 | — | 0.33 | 0.27 |
| $\tilde{F}_{3,3}$ | −0.13 | 0.62 | 1.04 | 0.92 | 0.05 |
| $\tilde{q}$ | −0.13 | 0.80 | 1.04 | 0.81 | 0.16 |
| $\tilde{\tau}_{13}$ | −0.18 | 0.68 | 0.41 | 0.21 | 0.18 |
| $\tilde{\tau}_{23}$ | — | 0.50 | — | 0.25 | 0.11 |
| $\tilde{\tau}_{12}$ | −0.01 | 0.69 | 0.02 | 0.12 | 0.14 |
| $\tilde{\tau}_{11}$ | 0.10 | 0.79 | 0.02 | 0.11 | 0.14 |
| $\tilde{\tau}_{22}$ | −0.11 | 0.69 | −0.05 | 0.16 | 0.06 |
| $\tilde{\tau}_{33}$ | 0.01 | 0.59 | −0.89 | 0.19 | 0.28 |
| $\tilde{\tau}_{11,1}$ | — | 0.57 | — | 0.12 | 0.14 |
| $\tilde{\tau}_{12,2}$ | — | 0.67 | — | 0.11 | 0.18 |
| $\tilde{\tau}_{13,3}$ | 0.16 | 0.95 | 0.41 | 0.42 | 0.04 |
| $\tilde{a}_1$ | 0.16 | 1.21 | 0.41 | 0.37 | 0.08 |
| $\tilde{\tau}_{21,1}$ | — | 0.52 | — | 0.09 | 0.01 |
| $\tilde{\tau}_{22,2}$ | — | 0.63 | — | 0.15 | 0.10 |
| $\tilde{\tau}_{23,3}$ | — | 0.74 | — | 0.45 | 0.00 |
| $\tilde{a}_2$ | — | 1.02 | — | 0.38 | 0.02 |
| $\tilde{\tau}_{31,1}$ | — | 0.47 | — | 0.17 | 0.09 |
| $\tilde{\tau}_{32,2}$ | — | 0.47 | — | 0.17 | 0.07 |
| $\tilde{\tau}_{33,3}$ | 0.00 | 1.08 | 5.88 | 0.19 | 0.26 |
| $\tilde{a}_3$ | 0.00 | 1.36 | 5.88 | 0.12 | 0.26 |

of SGS energy, and in capturing the mean horizontal SGS temperature flux, due to the failure of the eddy-viscosity model of that flux (Wyngaard et al. 1971). These deficiencies in the SGS model, we hypothesize, can mask the effects of improved resolution of the structure of resolvable-scale surface fluxes.

### c. Results with improved subgrid-scale model

Mason and Thomson (1992) found that adding stochastic fluctuations to the SGS stress divergence improved the nondimensional mean shear in a neutral boundary layer calculated through LES. These fluctuations simulate the local transfer of energy from unresolved to resolved scale, or ''backscatter,'' in the Smagorinsky SGS closure. We implemented this modification to the SGS model used in Moeng's code along with the surface-flux conservation equations.

Moeng's code uses the SGS model proposed by Deardorff (1980) in which the subgrid-scale energy, $e = (u_i^s u_i^s)^r/2$, is calculated explicitly and used as the velocity scale for the SGS eddy diffusivity ($\tilde{K}$):

$$\tilde{\tau}_{ij}^r = -2\tilde{K}\tilde{S}_{ij}^r, \tag{85}$$

$$\tilde{K} = c_k\sqrt{e}\,l, \tag{86}$$

$$\tilde{Q}_i^r = -\frac{\tilde{K}}{\mathrm{Pr}}\frac{\partial\tilde{\theta}^r}{\partial x_i}, \tag{87}$$

where $\tilde{S}_{ij}^r$ is the resolvable strain rate tensor, $c_k$ is a constant, $l$ is the length scale of unresolved eddies, and Pr is the turbulent Prandtl number. Following the development of Mason and Thomson, we added a white-noise random acceleration, $a_i$, and a random temperature source, $q$, to the resolvable-scale equations:

$$\frac{\partial\tilde{u}_i^r}{\partial t} = \cdots - \frac{\partial\tilde{\tau}_{ij}^r}{\partial x_j} + a_i, \tag{88}$$

$$\frac{\partial\tilde{\theta}^r}{\partial t} = \cdots - \frac{\partial\tilde{Q}_j^r}{\partial x_j} + q, \tag{89}$$

to account for stochastic backscatter. To satisfy continuity $a_i$ was taken to be the curl of another random vector: $a_i = \epsilon_{ijk}b_{k,j}$. As indicated by Mason and Thomson, this random forcing adds a production rate $\overline{a_i a_i}\Delta t$ to the resolved-scale kinetic energy equation and $2\overline{q^2}\Delta t$ to the equation for resolved-scale temperature variance, where $\Delta t$ is the time step. Mason and Thomson show that when the filter scale is of the order of the scale of

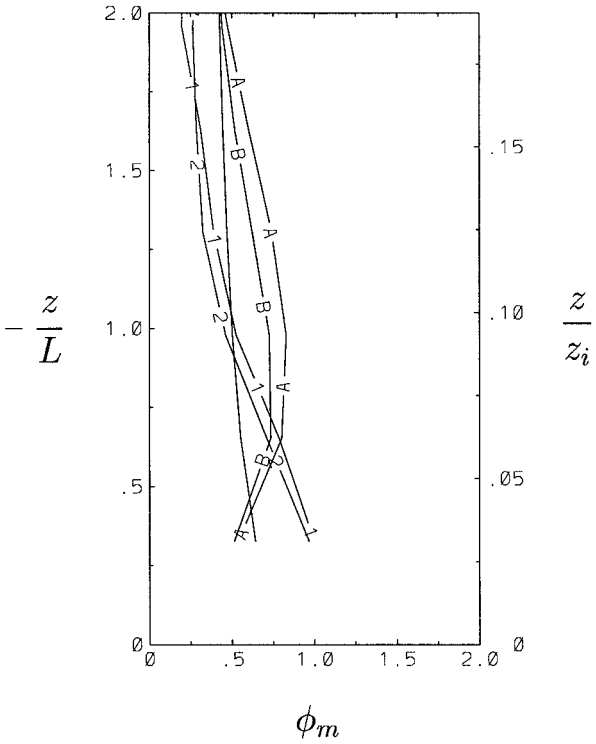


FIG. 7. Effect of SGS model and lower boundary conditions on the nondimensional mean shear. Curves 1 and 2 are from the original SGS model (without backscatter) and curves A and B from the modified SGS model (with backscatter). In both sets, the first curve is based on surface-exchange coefficients and the second on the surface flux equations.

the unresolved eddies, the mean backscatter of resolved-scale kinetic energy due to stochastic fluctuations in unresolved eddies is $c_b\epsilon$, where $\epsilon$ is the ensemble-average dissipation rate and $c_b = 1.4$; the mean backscatter of resolved-scale temperature variance is $2c_{b\theta}\chi$, where $\chi$ is the destruction rate of one-half temperature variance and $c_{b\theta} = 0.45$. The random components $b_i$ and $q$ are scaled such that

$$\overline{a_i a_i}\,\Delta t = c_b\epsilon, \tag{90}$$

$$\overline{q^2}\,\Delta t = c_{b\theta}\chi. \tag{91}$$

We increased the constant $c_k$ in (86) to $(1 + c_b)c_k$ to account for the additional production of resolved-scale kinetic energy. The turbulent Prandtl number in (87) was increased by a factor of $(1 + c_b)/(1 + c_{b\theta})$ to account for the additional production of resolved-scale temperature variance. The length scale $l$ in (86) was taken to be the minimum of $\Delta$, the grid scale, and $kz/c_k$, where $k$ is the von Kármán constant and $z$ is the distance from the surface.

Figure 7 shows the effect of the SGS model and lower boundary conditions on the $\phi_m$ profile in the $128^2 \times 64$ simulation of the moderately convective boundary layer. The original SGS model and drag coefficients overestimate $\phi_m$ at the first grid point ($z/z_i \approx 0.03$) by 50%. Use of surface-flux conservation equations with the original SGS model makes a marginal improvement. The modified SGS model (with stochastic backscatter) with the drag coefficients gives a smooth profile for $\phi_m$, although it is not entirely in agreement with the observed profile. The simulated value increases with $z/L$ before falling off, while the observed profile decreases monotonically. Our results are not in complete agreement with those of Mason and Thomson, presumably due to three factors: first, we are simulating a moderately convective boundary layer (with both buoyancy and shear effects) while their work concerned neutral boundary layers; second, we use a $128^2 \times 64$ mesh, whereas Mason and Thomson used a much finer vertical mesh compared to the horizontal mesh; finally, some of the parameters used in our implementation of the stochastic-backscatter model are different from those of Mason and Thomson. Nevertheless, we infer from these results that the subgrid-scale model does have a significant influence on the mean structure of the surface layer. Use of surface-flux conservation equations along with the stochastic backscatter model makes a marginal improvement. We conclude that the improved lower boundary conditions need a compatible subgrid-scale model to make better predictions of atmospheric surface layers.

## 7. Summary and conclusions

We argued physically and showed through analysis of observations and LES data that the local surface-exchange coefficient relating the resolvable-scale surface flux to resolvable-scale properties of the overlying flow is a random variable. Its fluctuation level increases with $z/\Delta$, where $z$ is height above the surface and $\Delta$ is the spatial scale of the filter that separates fields into resolvable-scale and subgrid-scale parts. As $z/\Delta \to 0$, the surface-exchange coefficient approaches its traditional definition.

An alternative to using a local surface-exchange coefficient to diagnose the resolvable-scale surface flux is predicting that flux through its conservation equation. We showed that near the surface this flux is dominated by the s–s component and we derived the equation for that component. We used the surface-layer spectral model of Peltier et al. (1996) to develop scaling expressions for the partitioning of the variances of surface-layer fields between the resolvable and subgrid-scale components. We used these scaling expressions to simplify the flux conservation equations in three limits.

For high aspect ratio grids, $z_1/\Delta \ll 1$, the surface-flux conservation equation is in a state of local grid volume equilibrium and the mean surface-exchange coefficient can be used locally, as is generally done in LES. For smaller aspect ratio grids it has horizontal advection and time-change terms, consistent with the appearance of fluctuations in the local surface-exchange coefficient in this regime. As the grid aspect ratio approaches unity, the flux conservation equation gains a production term proportional to the convergence of hor-

izontal velocity near the surface. The observed fluctuations in the local surface-exchange coefficient in this regime are quite large.

Based on Bradshaw's (1969) suggestion that horizontal inhomogeneity of the surface layer causes the local mean gradient of a transported quantity to deviate from its equilibrium value, we proposed a simple closure for the flux conservation equations and implemented them in the Moeng (1984) LES code.

Use of the surface flux conservation equations yields slight improvements in the nondimensional mean shear, mean potential temperature gradient, and vertical-velocity variance profiles. The commonly observed kink in the mean shear and temperature gradient profiles predicted by Smagorinsky-based SGS models at $z \approx \Delta$ is reduced. This improvement, however, is not substantial.

We showed through highly resolved LES that the Smagorinsky-based SGS models perform poorly in the atmospheric surface layer; a better SGS model is needed. We are currently extending the present analysis to derive conservation equations for SGS stresses and fluxes in the atmospheric surface layer, which, combined with dynamic lower boundary conditions, will hopefully make significant improvements in the LES predictions of atmospheric surface-layer structure.

*Acknowledgments.* We are grateful to T. Horst and G. Maclean of NCAR SSSF for kindly providing ASTER data from the STORMFEST experiment; to Andrew R. Brown of U.K. Meteorological Office for helpful discussions on stochastic backscatter; and to J. Brasseur, P. Mourad, and P. Sullivan for making helpful suggestions on the manuscript. This work was supported by Army Research Office Grant DAAL03-92-G-0117 and by Office of Naval Research Grant N00014-92-J-1688.

## APPENDIX A

## Simplifying the Resolvable-Scale Surface Scalar Flux Budget

Deriving the budget of resolvable-scale surface scalar flux as indicated in (23) yields

$$
\begin{aligned}
\frac{\partial}{\partial t}\tilde{F}^r_0 \approx\ & -((u^r_{3,j}u^r_j)^s c^s)^r && \text{resolvable shear, cross flux interaction} && \text{(RSCFI)}\\
& -((c^r_{,j}u^r_j)^s u^s_3)^r && \text{resolvable gradient, cross stress interaction} && \text{(RGCSI)}\\
& -((u^r_{3,j}u^s_j)^s c^s)^r && \text{resolvable-scale shear production} && \text{(RSSP)}\\
& -((u^r_j u^s_{3,j})^s c^s + (u^r_j c^s_{,j})^s u^s_3)^r && \text{large-scale advection} && \text{(LSA)}\\
& -U_j\tilde{F}^r_{0,j} && \text{mean advection} && \text{(MA)}\\
& -((u^s_j u^s_{3,j})^s c^s + (u^s_j c^s_{,j})^s u^s_3)^r && \text{small-scale advection} && \text{(SSA)}\\
& -((c^r_{,j}u^s_j)^s u^s_3)^r && \text{resolvable-scale gradient production} && \text{(RSGP)}\\
& -C_{,3}(u^s_3 u^s_3)^r && \text{mean-gradient production} && \text{(MGP)}\\
& +\frac{g}{T_0}(\theta^s c^s)^r && \text{buoyant production} && \text{(BP)}\\
& -(p^s_{,3}c^s)^r && \text{pressure destruction} && \text{(PD)}\\
& +\gamma(c^s_{,jj}u^s_3)^r + \nu(u^s_{3,jj}c^s)^r && \text{molecular terms} && \text{(M).}
\end{aligned}
\tag{A1}
$$

We can simplify a number of the terms in (A1). We rewrite the resolvable-scale shear production term (RSSP) as

$$\text{RSSP} = -[(u^r_{3,j}u^s_j)^s c^s]^r = -[(u^r_{3,j}u^s_j)c^s]^r + [(u^r_{3,j}u^s_j)^r c^s]^r. \tag{A2}$$

The term on the far right has the form $(a^r b^s)^r$. The wavenumber components of $a^r$ have magnitudes between 0 and $\kappa_c$. The wavenumber components of $b^s$ have magnitudes greater than $\kappa_c$. Let us write this symbolically as

$$(a^r b^s)^r = \{[0,\ \kappa_c](\kappa_c,\ \infty]\}^r = [0,\ \kappa_c]. \tag{A3}$$

In our notation, brackets mean that the set's end point is included in the range and parentheses mean that the set's end point is not included in the range. The wavenumber components of $a^r b^s$ are the vector sum of all those of $a^r$ and $b^s$. Therefore wavenumbers of $b^s$ larger than $2\kappa_c$ cannot contribute to $(a^r b^s)^r$, so we can write (A3) as

$$(a^r b^s)^r = \{[0,\ \kappa_c](\kappa_c,\ 2\kappa_c]\}^r. \tag{A4}$$

The variable $b$ is the temperature field, whose dominant

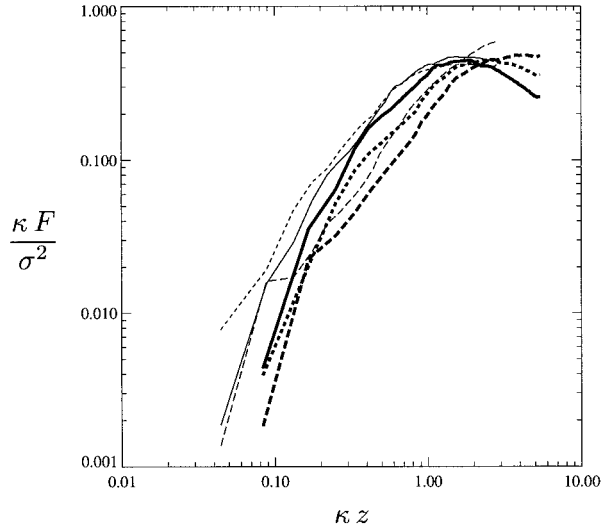


FIG. A1. The spectra of vertical temperature flux (long dashes), horizontal temperature flux (short dashes), and vertical velocity (solid) from high-resolution LES at $z = 35$ m (fine) and 66 m (bold) for $-z_i/L \simeq 65$.

wavenumbers have magnitudes of the order of $1/z$ (Peltier et al. 1996). Thus, as $\kappa_c z \to 0$, there are no modes of $b$ in the range $(\kappa_c, 2\kappa_c]$ so that $(a^r b^s)^r$ vanishes, and we can write

$$(a^r b^s)^r \ll (ab^s)^r \quad \text{as} \quad \kappa_c z \to 0. \tag{A5}$$

We will refer to the development that leads to (A5) as the *scale-separation* argument.

We can now rewrite (A2) as

$$\text{RSSP} = -[u^r_{3,j}(u^s_j c^s)]^r = -[u^r_{3,j}(u^s_j c^s)^r]^r - [u^r_{3,j}(u^s_j c^s)^s]^r. \tag{A6}$$

In order to proceed we need to know the shape of the spectrum of $u^s_j c^s$. We calculated it for $j = 1$ and $j = 3$ from high-resolution ($256^3$) LES data. The results, shown in Fig. A1, indicate that the spectrum of $u^s_j c^s$ is like that of $u_3$ in that it peaks at $\kappa \sim 1/z$. Thus, we can use the scale-separation argument to drop the second term on the right side of (A6). This yields

$$\text{RSSP} \to -[u^r_{3,j}(u^s_j c^s)^r]^r \quad \text{as} \quad \kappa_c z \to 0. \tag{A7}$$

We can rewrite the large-scale advection terms as

$$\begin{aligned}\text{LSA} &= -[(u^r_j u^s_{3,j})^s c^s + (u^r_j c^s_{,j})^s u^s_3]^r \\ &= -[(u^r_j u^s_{3,j})c^s + (u^r_j c^s_{,j})u^s_3]^r \\ &\quad + [(u^r_j u^s_{3,j})^r c^s + (u^r_j c^s_{,j})^r u^s_3]^r. \end{aligned} \tag{A8}$$

We can drop the second pair of terms through the scale-separation argument. Rewriting the first pair gives

$$\begin{aligned}\text{LSA} &= -[u^r_j (u^s_3 c^s)_{,j}]^r \\ &= -[u^r_j (u^s_3 c^s)^r_{,j}]^r + [u^r_j (u^s_3 c^s)^s_{,j}]^r. \end{aligned} \tag{A9}$$

The scale-separation argument allows us to drop the second term in (A9), yielding finally

$$\text{LSA} = -[u^r_j (u^s_3 c^s)^r_{,j}]^r = -[u^r_j \tilde{F}^r_{3,j}]^r. \tag{A10}$$

The small-scale advection term is

$$\begin{aligned}\text{SSA} &= -[(u^r_j u^s_{3,j})^s c^s + (u^s_j c^s_{,j})^s u^s_3]^r \\ &= -[(u^s_j u^s_{3,j})c^s + (u^s_j c^s_{,j})u^s_3]^r \\ &\quad + [(u^s_j u^s_{3,j})^r c^s + (u^s_j c^s_{,j})^r u^s_3]^r. \end{aligned} \tag{A11}$$

We drop the second pair of terms through the scale-separation argument and obtain

$$\text{SSA} = -[u^s_j u^s_3 c^s]^r_{,j}. \tag{A12}$$

The resolvable-scale gradient production term is

$$\begin{aligned}\text{RSGP} &= -[(c^r_j u^s_j)^s u^s_3]^r \\ &= -[(c^r_j u^s_j)u^s_3]^r + [(c^r_j u^s_j)^r u^s_3]^r. \end{aligned} \tag{A13}$$

Dropping the second term through the scale-separation argument yields

$$\begin{aligned}\text{RSGP} &= -[c^r_j u^s_j u^s_3]^r \\ &= -[c^r_j (u^s_j u^s_3)^r]^r - [c^r_j (u^s_j u^s_3)^s]^r. \end{aligned} \tag{A14}$$

Dropping the second term through the scale-separation argument then finally yields

$$\text{RSGP} = -[c^r_j (u^s_j u^s_3)^r]^r. \tag{A15}$$

The molecular terms can be rewritten

$$\begin{aligned}&\gamma(c^s_{,jj} u^s_3)^r + \nu(u^s_{3,jj} c^s)^r \\ &\quad = (\nu + \gamma)(c^s u^s_3)^r_{,jj} - \nu(c^s_{,j} u^s_3)^r_{,j} - \gamma(c^s u^s_{3,j})^r_{,j} \\ &\qquad - (\nu + \gamma)(c^s_{,j} u^s_{3,j})^r. \end{aligned} \tag{A16}$$

We can drop these terms on the basis of arguments used by Wyngaard (1982) for the analogous terms in the Reynolds flux budget. The first term, molecular diffusion, and the second are negligible because of the large Reynolds and Peclet numbers above the molecular sublayer. The third term, molecular destruction, is assumed negligible on the grounds of local isotropy (Wyngaard et al. 1971).

Finally, we drop a mean-shear production term $-U_{3,j}(u^s_j c^s)^r$ from (A1) because it vanishes under horizontally homogeneous conditions. The simplified budget reads

$$\begin{aligned}\frac{\partial}{\partial t}\tilde{F}^r_0 \approx\ & -((u^r_{3,j} u^r_j)^s c^s)^r && \text{resolvable shear, cross flux interaction} && \text{(RSCFI)} \\ & -((c^r_{,j} u^r_j)^s u^s_3)^r && \text{resolvable gradient, cross stress interaction} && \text{(RGCSI)} \\ & -(u^r_{3,j}(u^s_j c^s)^r)^r && \text{resolvable-scale shear production} && \text{(RSSP)}\end{aligned}$$

$$
\begin{aligned}
&- (u_j^r \tilde{F}_3^r)_{,j}^r && \text{large-scale advection} && \text{(LSA)}\\
&- U_j \tilde{F}_{0,j}^r && \text{mean advection} && \text{(MA)}\\
&- (u_j^s u_3^s c^s)_{,j}^r && \text{small-scale advection} && \text{(SSA)}\\
&- (c_{,j}^r (u_j^s u_3^s)^r)^r && \text{resolvable-scale gradient production} && \text{(RSGP)}\\
&- C_{,3} (u_3^s u_3^s)^r && \text{mean-gradient production} && \text{(MGP)}\\
&+ \frac{g}{T_0} (\theta^s c^s)^r && \text{buoyant production} && \text{(BP)}\\
&- (p_{,3}^s c^s)^r && \text{pressure destruction} && \text{(PD).}
\end{aligned} \tag{A17}
$$

## APPENDIX B

### The Cross Components of SGS Flux

We showed in Eq. (17) that with wave-cutoff filtering the SGS flux can be written

$$\tilde{F}_3^r = (c^r u_3^s + c^s u_3^r + c^s u_3^s)^r. \tag{B1}$$

We designate $(c^r u_3^s)^r$ and $(c^s u_3^r)^r$ as the cross components. By the arguments in section 3 of the paper, the contributing wavenumber ranges of $u_3^s$ and $c^s$ here are $\kappa_c < \kappa \le 2\kappa_c$. We can therefore estimate the magnitude of the cross fluxes as

$$(c^r u_3^s)^r \sim c^r \delta u_3^s, \qquad c^s u_3^r \sim \delta c^s u_3^r, \tag{B2}$$

where $\delta u_3^s$ means the rms value of $u_3^s$ when its wavenumbers are restricted to the range $\kappa_c < \kappa \le 2\kappa_c$. Since, in general, we can write

$$
\begin{aligned}
\overline{(\delta f^s)^2} &= \int_{\kappa_c}^{2\kappa_c} E(\kappa)\, d\kappa\\
&= \int_0^{2\kappa_c} E(\kappa)\, d\kappa - \int_0^{\kappa_c} E(\kappa)\, d\kappa,
\end{aligned} \tag{B3}
$$

it follows that

$$(\delta f^s)^2 = [f^r(2\kappa_c)]^2 - [f^r(\kappa_c)]^2. \tag{B4}$$

Using (33), (36), (41), and (43) in (B4) then yields

$$\delta u_3^s \sim u_3^r, \qquad \delta c^s \sim c^r. \tag{B5}$$

Our scaling estimates for the cross fluxes are then

$$(c^r u_3^s)^r \sim c^r u_3^r, \qquad (c^s u_3^r)^r \sim c^r u_3^r \tag{B6}$$

so that each is of the order of the resolvable-scale flux. It follows from our scaling estimates that

$$\text{cross flux} \sim F_0 \left(\frac{z}{\Delta}\right)^3, \quad \text{neutral and free convection.} \tag{B7}$$

Thus, we can write for the entire stability range

$$\frac{\text{cross flux}}{\text{s–s flux}} \sim \left(\frac{z}{\Delta}\right)^3. \tag{B8}$$

This confirms that the cross flux is negligible sufficiently close to the surface.

## APPENDIX C

### Extension to Resolvable-Scale Surface Stress

*a. The resolvable-scale surface stress budget*

Filtering the momentum Eq. (10) yields the evolution equation for its resolvable-scale part:

$$\frac{\partial \tilde{u}_i^r}{\partial t} + (\tilde{u}_{i,j}^r \tilde{u}_j^r)^r + \tilde{R}_{ij,j}^r = -\tilde{p}_{,i}^r + \frac{g}{T_0} \tilde{\theta}^r \delta_{3i}, \tag{C1}$$

where the SGS stress tensor $\tilde{R}_{ij}^r$ is

$$\tilde{R}_{ij}^r = (\tilde{u}_i^r \tilde{u}_j^s + \tilde{u}_i^s \tilde{u}_j^r + \tilde{u}_i^s \tilde{u}_j^s)^r - \nu(\tilde{u}_{i,j}^r + \tilde{u}_{j,i}^r). \tag{C2}$$

We again neglect the molecular contribution and define the *deviatoric* SGS stress tensor:

$$\tilde{\tau}_{ij}^r = \tilde{R}_{ij}^r - \frac{\tilde{R}_{kk}^r}{3} \delta_{ij}. \tag{C3}$$

We write the shear stress components $\tilde{\tau}_{13}^r$ and $\tilde{\tau}_{23}^r$ near the surface as $\tilde{\tau}_{0k}^r$. Through our scaling arguments, they are good surrogates for the resolvable-scale surface shear stress. From (C2) they are the sum of ''cross'' and ''s–s'' parts:

$$\tilde{\tau}_{0k}^r = (u_k^r u_3^s + u_k^s u_3^r)^r + (u_k^s u_3^s)^r = \tilde{C}_{0k}^r + \tilde{S}_{0k}^r, \qquad k = 1, 2. \tag{C4}$$

Deriving the budget of $\tilde{S}_{0k}^r$ as indicated in (23) yields

$$
\begin{aligned}
\frac{\partial}{\partial t} \tilde{S}_{0k}^r \approx\ & -((u_{3,j}^r u_j^r)^s u_k^s)^r && \text{resolvable shear, cross flux interaction} && \text{(RSCFI)}\\
& - ((u_{k,j}^r u_j^r)^s u_3^s)^r && \text{resolvable gradient, cross stress interaction} && \text{(RGCSI)}
\end{aligned}
$$

$$
\begin{aligned}
&-((u^r_{3,j}u^s_j)^s u^s_k)^r && \text{resolvable-scale shear production} && \text{(RSSP)}\\
&-((u^r_j u^s_{3,j})^s u^s_k + (u^r_j u^s_{k,j})^s u^s_3)^r && \text{large-scale advection} && \text{(LSA)}\\
&-U_j \tilde{S}^r_{0k,j} && \text{mean advection} && \text{(MA)}\\
&-((u^s_j u^s_{3,j})^s u^s_k + (u^s_j u^s_{k,j})^s u^s_3)^r && \text{small-scale advection} && \text{(SSA)}\\
&-((u^r_{k,j}u^s_j)^s u^s_3)^r && \text{resolvable-scale gradient production} && \text{(RSGP)}\\
&-U_{k,3}(u^s_3 u^s_3)^r && \text{mean-gradient production} && \text{(MGP)}\\
&+\frac{g}{T_0}(\theta^s u^s_k)^r && \text{buoyant production} && \text{(BP)}\\
&-(p^s_{,3}u^s_k)^r - (p^s_{,k}u^s_3)^r && \text{pressure destruction} && \text{(PD).}
\end{aligned}
\tag{C5}
$$

The scaling procedure discussed in the text yields the estimates, shown in Table C1, of the magnitudes of the terms in (C5).

### b. The constant-SGS-stress layer

To verify the feasibility of solving the surface-stress conservation equation away from the surface, we evaluate the ratio of the difference between the surface stress and the stress at height $z$ to the fluctuation in stress at height $z$. This ratio is approximately given by

$$\frac{z}{\tau_{h3}}\frac{\partial \tau_{h3}}{\partial z}. \tag{C6}$$

We estimate the vertical stress gradient from the resolvable-scale horizontal momentum equation by assuming the inertial term to be of the leading order. Using our scaling estimates in section 4, we find

$$
\begin{aligned}
\frac{z}{\tau_{h3}}\frac{\partial \tau_{h3}}{\partial z} &\approx \left(\frac{z}{\Delta}\right)^3 : \text{neutral},\\
&\approx \left(\frac{z}{\Delta}\right)^{2/3}\left(\frac{\Delta}{z_i}\right)^{1/3}\left(1-\left[\frac{z}{\Delta}\right]^{4/3}\right)^{-1}\\
&\quad : \text{free convection}.
\end{aligned}
\tag{C7}
$$

We conclude that for a sufficiently small $z/\Delta$ there exists a constant-SGS-stress layer such that the SGS stress at height $z$ is a reliable surrogate for the surface stress.

In a similar analysis, Mason and Thomson (1992) assumed that as the surface is approached the vertical stress gradient is balanced by the horizontal pressure gradient, which they estimated to be roughly independent of height. Their estimate of vertical stress gradient, therefore, differs from ours. The conclusion regarding the constant-SGS-stress layer, however, still holds albeit for a smaller $z/\Delta$. The discrepancy can only be resolved through direct numerical simulations.

### c. The cross stresses

As shown in appendix B, the cross stresses are of order

TABLE C1. Scaling of terms in the budget of surface stress.

| | |
|---|---|
| RSCFI: | $((u^r_{3,j}u^r_j)^s u^s_k)^r \sim u^r_{3,j}u^r_j \delta u^s_h$ |
| RGCSI: | $((u^r_{k,j}u^r_j)^s u^s_3)^r \sim u^r_{h,j}u^r_j \delta u^s_3$ |
| RSSP: | $((u^r_{3,j}u^s_j)^s u^s_k)^r \sim u^r_{3,j}u^s_j u^s_h$ |
| LSA: | $((u^r_j u^s_{3,j})^s u^s_k + (u^r_j u^s_{k,j})^s u^s_3)^r \sim u^r_j (u^s_3 u^s_k)^r_{,j}$ |
| MA: | $U_j \tilde{S}^r_{k3,j} \sim u^r_{h,h} S^r_{k3}$ |
| SSA: | $((u^s_j u^s_{3,j})^s u^s_k + (u^s_j u^s_{k,j})^s u^s_3)^r \sim (u^s_j u^s_3 u^s_h)_{,j}$ |
| RSGP: | $((u^r_{k,j}u^s_j)^s u^s_3)^r \sim u^r_{k,j}u^s_j u^s_3$ |
| MGP: | $U_{k,3}(u^s_3 u^s_3)^r \sim U_{1,3}u^s_3 u^s_3$ |
| BP: | $\frac{g}{T_0}(\theta^s u^s_k)^r \sim \frac{g}{T_0}\theta^s u^s_k$ |
| PD: | $(p^s_{,3}u^s_k)^r + (p^s_{,k}u^s_3)^r \sim p^s_{,3}u^s_k$ |

| | Neutral $\left(\text{units of } u_*^2\frac{u_*}{z}\right)$ | | Free convection $\left(\text{units of } u_f^2\frac{u_f}{z}\right)$ | |
|---|---|---|---|---|
| Term | $j = 1, 2$ | $j = 3$ | $j = 1, 2$ | $j = 3$ |
| RSCFI | $\left(\frac{z}{\Delta}\right)^5$ | $\left(\frac{z}{\Delta}\right)^5$ | $\left(\frac{z}{\Delta}\right)\left(\frac{z_i}{\Delta}\right)^{1/3}$ | $\left(\frac{z}{\Delta}\right)$ |
| RGCSI | $\left(\frac{z}{\Delta}\right)^5$ | $\left(\frac{z}{\Delta}\right)^5$ | $\left(\frac{z}{\Delta}\right)\left(\frac{z_i}{\Delta}\right)^{1/3}$ | $\left(\frac{z}{\Delta}\right)^2$ |
| RSSP | $\left(\frac{z}{\Delta}\right)^3$ | $\left(\frac{z}{\Delta}\right)^2$ | $\left(\frac{z}{\Delta}\right)$ | $\left(\frac{z}{\Delta}\right)^{2/3}$ |
| LSA | $\left(\frac{z}{\Delta}\right)^3\left(\frac{u_*}{U_1}\right)$ | $\left(\frac{z}{\Delta}\right)^5$ | $\left(\frac{z}{\Delta}\right)^{2/3}\left(\frac{z_i}{\Delta}\right)^{1/3}$ | $\left(\frac{z}{\Delta}\right)\left(\frac{z_i}{\Delta}\right)^{1/3}$ |
| MA | $\left(\frac{z}{\Delta}\right)^2$ | 0 | 0 | 0 |
| SSA | $\left(\frac{z}{\Delta}\right)$ | 1 | $\left(\frac{z}{\Delta}\right)$ | 1 |
| RSGP | $\left(\frac{z}{\Delta}\right)^2$ | $\left(\frac{z}{\Delta}\right)$ | $\left(\frac{z}{\Delta}\right)^{2/3}$ | $\left(\frac{z}{\Delta}\right)^{2/3}$ |
| MGP | 1 | | 0 | |
| BP | 0 | | 1 | |
| PD | 1 | | 1 | |

$$(u_k^r u_3^s)^r \sim u_h^r \delta u_3^s \sim u_h^r u_3^r,$$
$$(u_k^s u_3^r)^r \sim \delta u_h^s u_3^r \sim u_h^r u_3^r \quad \text{(neutral)},$$
$$\sim u_h^s u_3^r \quad \text{(free convection)}. \quad \text{(C8)}$$

Our scaling estimates in conjunction with (C8) show that the dominant contributor to the cross stress is $(u_k^r u_3^s)^r \sim u_h^r \delta u_3^s \sim u_h^r u_3^r$. Thus, we can write

$$\text{cross stress} \sim u_*^2 \left(\frac{z}{\Delta}\right)^3 \quad \text{(neutral)},$$
$$u_f^2 \left(\frac{z}{\Delta}\right)^{1/3} \left(\frac{z_i}{\Delta}\right)^{1/3} \quad \text{(free convection)}. \quad \text{(C9)}$$

We estimate the magnitude of the s–s component of the SGS stress as

$$\text{s–s stress} = (u_k^s u_3^s)^r \sim u_h^s u_3^s \sim u_*^2 \quad \text{(neutral)},$$
$$u_f^2 \left(\frac{z}{\Delta}\right)^{-1/3} \quad \text{(free convection)}, \quad \text{(C10)}$$

From (C9) and (C10) we have

$$\frac{\text{cross stress}}{\text{s–s stress}} \sim \left(\frac{z}{\Delta}\right)^3 \quad \text{(neutral)},$$
$$\left(\frac{z_i}{\Delta}\right)^{1/3} \left(\frac{z}{\Delta}\right)^{2/3} \quad \text{(free convection)}. \quad \text{(C11)}$$

Equation (C11) confirms that the cross stress is negligible sufficiently close to the surface.

Equation (C11) also indicates that under free-convection conditions the cross stress can be of the order of the s–s stress when

$$\left(\frac{z_i}{\Delta}\right)^{1/3} \left(\frac{z}{\Delta}\right)^{2/3} \sim 1, \quad \text{or} \quad \frac{z}{\Delta} \sim \left(\frac{\Delta}{z_i}\right)^{1/2}. \quad \text{(C12)}$$

For typical values of $\Delta/z_i$ (1/10 to 1/100, say) (C12) indicates that in free convection the cross stress is as important as the s–s stress when $z/\Delta \sim 0.1$ to 0.3. For larger $z/\Delta$ values, the cross term can be the dominant contributor to SGS stress. This is unlike the situation for scalar flux, for which we showed (appendix B) that the cross components are quite small.

### *d. The surface stress budget for $z_1/\Delta \ll 1$*

When $z/\Delta \ll 1$ only the $O(1)$ terms in (C5) are significant so the streamwise stress budget reduces to

$$\frac{\partial}{\partial t}\tilde{S}_{01}^r \approx 0 \approx -[(u_3^s u_{3,3}^s)^s u_1^s + (u_3^s u_{1,3}^s)^s u_3^s]^r$$
$$- U_{1,3}(u_3^s u_3^s)^r + \frac{g}{T_0}(\theta^s u_1^s)^r$$
$$- (p_{,3}^s u_1^s)^r - (p_{,1}^s u_3^s)^r. \quad \text{(C13)}$$

The $\kappa = 0$ component of this equation is the Reynolds budget of streamwise stress (Wyngaard et al. 1971).

The lateral stress budget for $z/\Delta \ll 1$ becomes

$$\frac{\partial}{\partial t}\tilde{S}_{02}^r \approx 0 \approx -[(u_3^s u_{3,3}^s)^s u_2^s + (u_3^s u_{2,3}^s)^s u_3^s]^r$$
$$+ \frac{g}{T_0}(\theta^s u_2^s)^r - (p_{,3}^s u_2^s)^r - (p_{,2}^s u_3^s)^r. \quad \text{(C14)}$$

The mean (the $\kappa = 0$ component) of each term in this equation vanishes, due to the symmetry about the $x_1$ axis. Thus, (C14) predicts zero mean lateral stress, as expected; however, fluctuations in the lateral stress are generated by small-scale advection, buoyancy, and the pressure term.

We argued in section 5 of the paper that when $z_1/\Delta \ll 1$ the turbulence in the first grid element is in local grid volume equilibrium. A closure for the resolvable-scale surface stress budgets (C13) and (C14) in this case is

$$\tilde{S}_{0k}^r = C_D(z_1/\tilde{L})[\tilde{s}^r(z_1)\tilde{u}_k^r(z_1)]^r.$$
$$(k = 1, 2; \qquad z_1/\Delta \ll 1). \quad \text{(C15)}$$

Here $C_D$ is the mean surface-exchange coefficient for momentum and $\tilde{s}^r$ is the resolvable-scale horizontal wind speed.

### *e. The surface stress budget for $z_1/\Delta < 1$*

Table C1 shows that in free convection there is not the clear separation in the order of the terms that existed for scalar flux. The next-order terms in (C5) are of order $(z/\Delta)^{2/3}$, but after that come a number of zero-mean, ''noise terms'' (e.g., RSCFI, RGCSI) of order $z/\Delta$.

Despite this lack of separation, the two budgets are similar in that the next-order terms are large-scale advection, resolvable-scale gradient production, and the vertical part of resolvable-scale shear production. We argued in the paper that the time-change term is of the order of advection, which we will take to include that by the mean velocity.

Rewriting the resolvable-scale gradient production term as we did for scalar flux and using the scale-separation argument (appendix A) gives

$$\text{RSGP} \approx -(u_{k,j}^r (u_j^s u_3^s)^r)^r. \quad \text{(C16)}$$

The scale-separation argument is inapplicable to the resolvable-scale shear production term due to the $u_k^s$ contained within it, so the term is

$$\text{RSSP} = -(u_{3,j}^r (u_j^s u_k^s)^r)^r - (u_{3,j}^r (u_j^s u_k^s)^s)^r + ((u_{3,j}^r u_j^s)^r u_k^s)^r. \quad \text{(C17)}$$

Only the first term in (C17) can be calculated, so we will drop the second and third, which are zero-mean ''noise'' terms, and write for its vertical part

$$\text{RSSP} \approx -(u_{3,3}^r (u_3^s u_k^s)^r)^r \simeq -(u_{3,3}^r \tilde{S}_{0k}^r)^r. \quad \text{(C18)}$$

The budget of $\tilde{S}_{0k}^r$ then becomes

$$\frac{\partial}{\partial t}\tilde{S}^r_{0k} + (\tilde{u}^r_h \tilde{S}^r_{0k})^r_{,h} + (u^r_{3,3}\tilde{S}^r_{0k})^r + [(u^s_3 u^s_{3,3})^s u^s_k + (u^s_3 u^s_{k,3})^s u^s_3]^r + (\tilde{u}^r_{k,j}(u^s_j u^s_3)^r)^r - \frac{g}{T_0}(\theta^s u^s_k)^r \approx -(p^s_{,3} u^s_k)^r - (p^s_{,k} u^s_3)^r. \quad \text{(C19)}$$

This is the counterpart to Eq. (74) for the surface scalar flux.

We showed in section 2 of this appendix that the cross contribution is relatively more important for stress than it is for scalar flux. Thus, when $z_1/\Delta$ is not very small so that a surface stress conservation equation rather than the usual surface-exchange expression is appropriate, it appears that the cross stress could also be significant. We showed that the dominant cross stress is $(u^r_k u^s_3)^r$, which in principle is inaccessible since it involves a subgrid-scale quantity. It has zero mean and we showed that its rms magnitude is of order $u^r_k u^r_3$, which is calculated in LES. We discuss the modeling of this term in section 6a.

## REFERENCES


Bardina, J., J. H. Ferziger, and W. C. Reynolds, 1983: Improved turbulence models based on large-eddy simulation of homogeneous, incompressible, turbulent flows. Tech. Rep. TF-19, Stanford University, Stanford, CA, 174 pp.

Bradshaw, P., 1969: Comments on ''On the relation between the shear stress and the velocity profile after change in surface roughness.'' *J. Atmos. Sci.,* **26,** 1353–1354.

Businger, J. A., J. C. Wyngaard, Y. Izumi, and E. F. Bradley, 1971: Flux-profile relationships in the atmospheric surface layer. *J. Atmos. Sci.,* **28,** 181–189.

Clark, R. A., J. H. Ferziger, and W. C. Reynolds, 1979: Evaluation of subgrid-scale models using an accurately simulated turbulent flow. *J. Fluid Mech.,* **91,** 1–16.

Cotton, W. R., R. L. Walko, K. R. Costigan, P. J. Flatau, and R. A. Pielke, 1993: Using the Regional Atmospheric Modeling System in the large-eddy-simulation mode: From inhomogeneous surfaces to cirrus clouds. *Large-Eddy Simulation of Complex Engineering and Geophysical Flows,* B. Galperin and S. Orszag, Eds., Cambridge University Press, 369–398.

Deardorff, J. W., 1970: A numerical study of three-dimensional turbulent channel flow at large Reynolds numbers. *J. Fluid Mech.,* **41,** 453–480.

——, 1980: Stratocumulus-capped mixed layers derived from a three-dimensional model. *Bound.-Layer Meteor.,* **18,** 495–527.

Kaimal, J. C., 1978: Horizontal velocity spectra in an unstable surface layer. *J. Atmos. Sci.,* **35,** 18–24.

Khanna, S., and J. G. Brasseur, 1996: Analysis of Monin–Obukhov similarity from large-eddy simulation. *J. Fluid Mech.,* **345,** 251–286.

Klemp, J. B., 1987: Dynamics of tornadic thunderstorms. *Annu. Rev. Fluid Mech.,* **19,** 369–402.

Leonard, A., 1974: Energy cascade in large eddy simulation of turbulent flows. *Advances in Geophysics,* Vol. 18A, Academic Press, 237–248.

Lilly, D. K., 1967: The representation of small-scale turbulence in numerical simulation experiments. *Proc. Tenth IBM Scientific Computing Symp. on Environmental Sciences,* IBM Thomas J. Watson Research Center, Yorktown Heights, NY, 195–210.

Lumley, J. L., and H. A. Panofsky, 1964: *The Structure of Atmospheric Turbulence.* Interscience, 239 pp.

Mason, P. J., and N. S. Callen, 1986: On the magnitude of the SGS eddy coefficient in LES of turbulent channel flows. *J. Fluid Mech.,* **162,** 439–462.

——, and D. J. Thomson, 1987: Large-eddy simulation of the neutral-static-stability planetary boundary layer. *Quart. J. Roy. Meteor. Soc.,* **113,** 413–443.

——, and ——, 1992: Stochastic backscatter in large-eddy simulations of boundary layers. *J. Fluid Mech.,* **242,** 51–78.

Moeng, C.-H., 1984: A large-eddy-simulation model for the study of planetary boundary layer turbulence. *J. Atmos. Sci.,* **41,** 2052–2062.

Nieuwstadt, F. T. M., P. J. Mason, C.-H. Moeng, and U. Schumann, 1993: Large-eddy simulation of the convective boundary layer: A comparison of four computer codes. *Turbulent Shear Flows,* F. Durst, R. Friedrich, B. E. Launder, F. W. Schmidt, U. Schumann, and J. H. Whitelaw, Eds., Vol. 8, Springer-Verlag, 343–368.

Panofsky, H. A., and J. A. Dutton, 1984: *Atmospheric Turbulence.* Wiley, 397 pp.

——, H. Tennekes, D. H. Lenschow, and J. C. Wyngaard, 1977: The characteristics of turbulent velocity components in the surface layer under convective conditions. *Bound.-Layer Meteor.,* **11,** 355–361.

Peltier, L. J., J. C. Wyngaard, S. Khanna, and J. G. Brasseur, 1996: Spectra in the unstable surface layer. *J. Atmos. Sci.,* **53,** 49–61.

Piomelli, U., W. H. Cabot, P. Moin, and S. Lee, 1991: Subgrid-scale backscatter in turbulent and transitional flows. *Phys. Fluids A,* **3,** 1766–1771.

Schumann, U., 1993: Large-eddy simulation of turbulent convection over flat and wavy surfaces. *Large-Eddy Simulation of Complex Engineering and Geophysical Flows,* B. Galperin and S. Orszag, Eds., Cambridge University Press, 399–421.

Stull, R., 1988: *An Introduction to Boundary Layer Meteorology.* Kluwer, 402 pp.

Sullivan, P., J. C. McWilliams, and C.-H. Moeng, 1994: A subgrid-scale model for large-eddy simulation of planetary boundary-layer flows. *Bound.-Layer Meteor.,* **71,** 247–276.

Tennekes, H., and J. L. Lumley, 1972: *A First Course in Turbulence.* The MIT Press, 300 pp.

Wyngaard, J. C., 1982: Planetary boundary layer modeling. *Atmospheric Turbulence and Air Pollution Modelling,* F. T. M. Nieuwstadt and H. van Dop, Eds., Reidel, 69–106.

——, 1988: Structure of the PBL. *Lectures on Air-Pollution Modeling,* A. Venkatram and J. C. Wyngaard, Eds., Amer. Meteor. Soc., 9–61.

——, and L. J. Peltier, 1996: Experimental micrometeorology in an era of turbulence simulation. *Bound.-Layer Meteor.,* **78,** 71–86.

——, O. R. Coté, and Y. Izumi, 1971: Local free convection, similarity, and the budgets of shear stress and heat flux. *J. Atmos. Sci.,* **28,** 1171–1182.